THE JOURNAL OF BIOLOGICAL CHEMISTRY VOL. 287, NO. 33, pp. 27380–27395, August 10, 2012

Peroxisomal Proteostasis Involves a Lon Family Protein That Functions as Protease and Chaperone*[S]

Received for publication, May 14, 2012, and in revised form, June 12, 2012 Published, JBC Papers in Press, June 25, 2012, 2012, DOI 10.1074/jbc.M112.381566

Magdalena Bartoszewska[‡1], Chris Williams[§], Alexey Kikhney[§], Łukasz Opaliński[‡1], Carlo W. T. van Roermund[¶], Rinse de Boer[‡2], Marten Veenhuis[‡], and Ida J. van der Klei[‡3]

From the [‡]Molecular Cell Biology, Groningen Biomolecular Sciences and Biotechnology Institute (GBB), University of Groningen, Kluyver Centre for Genomics of Industrial Fermentation, P. O. Box 11103, 9700CC Groningen, The Netherlands, [§]EMBL Hamburg Outstation, c/o DESY, Notkestrasse 85 22 603, Hamburg, Germany, and [¶]Laboratory Genetic Metabolic Diseases, Academic Medical Center, University of Amsterdam, Meibergdreef 9, 1105 AZ Amsterdam, The Netherlands

Background: A putative Lon protease has been identified in peroxisomes of various species (Pln).
Results: Pln is an ATP-dependent protease that digests unfolded substrates *e.g.* oxidatively damaged catalase-peroxidase, and displays chaperone-like activity, circumventing accumulation of protein aggregates in peroxisomes that compromise organelle function.
Conclusion: Pln is a bifunctional protein with chaperone and protease activities.
Significance: Pln is crucial for peroxisome proteostasis.

Proteins are subject to continuous quality control for optimal proteostasis. The knowledge of peroxisome quality control systems is still in its infancy. Here we show that peroxisomes contain a member of the Lon family of proteases (Pln). We show that Pln is a heptameric protein and acts as an ATP-fueled protease and chaperone. Hence, Pln is the first chaperone identified in fungal peroxisomes. In cells of a *PLN* deletion strain peroxisomes contain protein aggregates, a major component of which is catalase-peroxidase. We show that this enzyme is sensitive to oxidative damage. The oxidatively damaged, but not the native protein, is a substrate of the Pln protease. Cells of the *pln* strain contain enhanced levels of catalase-peroxidase protein but reduced catalase-peroxidase enzyme activities. Together with the observation that Pln has chaperone activity *in vitro*, our data suggest that catalase-peroxidase aggregates accumulate in peroxisomes of *pln* cells due to the combined absence of Pln protease and chaperone activities.

Functional proteins generally adapt a defined three-dimensional structure, designated their native fold. Nevertheless, they need to retain conformational flexibility to allow functioning, and as a consequence, they are only marginally thermodynamically stable macromolecules. Hence, preexisting folded proteins are at constant risk of being unfolded, especially at environmental stress conditions (1–3). Aberrantly folded polypeptides as well as folding intermediates expose hydrophobic residues that are normally buried in the native fold and are prone to trigger protein aggregation (4). Aggregation of misfolded protein species is linked with the perturbation of cellular functions, aging, and various human disorders (5). To circumvent this, cells evolved sophisticated protein quality control systems, among which are molecular chaperones that facilitate folding and refolding of polypeptides and proteolytic machines that remove misfolded conformers from the cellular interior (6). These systems are indispensable for protein homeostasis (proteostasis) in cells (7).

Yet little is known of protein quality control in peroxisomes. Despite their simple architecture, peroxisomes are important organelles that display an unprecedented diversity of functions depending on metabolic needs and external stimuli (8). They are crucial in man, manifested by the presence various inherited disorders (*i.e.* neonatal adrenoleukodystrophy, Zellweger syndrome, infantile Refsum's disease, rhizomelic chondrodysplasia punctata) caused by impairment of one or more peroxisomal functions (9, 10). The hallmark of peroxisomes is the metabolism of hydrogen peroxide that is generated as a byproduct of the organelle oxidative metabolism (11). Hydrogen peroxide can be the source of the most highly reactive and toxic form of reactive oxygen species, the hydroxyl radical (•OH), which is generated in the Fenton reaction (12). To cope with reactive oxygen species formation, peroxisomes contain a set of peroxide decomposing enzymes among which are catalase, peroxiredoxins, or peroxidases (11). Peroxisomes may import folded proteins and even oligomeric protein complexes (13) rendering these organelles attractive models to analyze the mechanisms involved in housekeeping of preexisting, folded proteins.

Recently, a conserved ATP-dependent Lon protease has been identified in peroxisomes (14, 15). The mitochondrial isoform of this protease was shown to represent the main quality control protease of the organelle matrix (16, 17). Mitochondrial Lon selectively degrades misfolded, unassembled, and damaged

* This work was supported in part by a Rubicon Fellowship (825.08.023) from the Netherlands Organization for Scientific Research (to C. W.).
[S] This article contains supplemental Figs. S1–S5.
[1] Supported by the Research Program of the Kluyver Centre for Genomics of Industrial Fermentation, which is part of the Netherlands Genomics Initiative/Netherlands Organization for Scientific Research.
[2] Supported by the Netherlands Organization for Scientific Research via the IBOS (Integration of Biosynthesis and Organic Synthesis) Programme of Advanced Chemical Technologies for Sustainability (ACTS) (project IBOS 053.63.011).
[3] To whom correspondence should be addressed: Molecular Cell Biology, Groningen Biomolecular Sciences and Biotechnology Institute (GBB), P. O. Box 11103, 9700CC Groningen, The Netherlands. Tel.: 31-50-363-2179; Fax: 31-50-363-8280; E-mail: I.J.van.der.klei@rug.nl.

TABLE 1
***P. chrysogenum* strains used in this study**

Strain	Genotype or characteristic	Reference
DS54465 GFP-SKL	DS54465 with integrated P_{gpdA}-*GFP.SKL*-T_{penDE} cassette at niaD locus, $AmdS^-$, chlorate-resistant	(50)
pln::GFP-SKL	DS54465 GFP-SKL with deletion of *pln* gene, chlorate-resistant, $AmdS^+$	This study
DsRed-SKL	DS17690 with integrated P_{pcbC}-*DsRed.SKL*-T_{penDE} cassette, $AmdS^-$	(26)
DsRed-SKL GFP.Pln	DsRed-SKL with integrated P_{gpdA}-mGFP.*pln*-T_{penDE}, $AmdS^+$	This study
DsRed-SKL GFP-catalase-peroxidase	DsRed-SKL with integrated P_{gpdA}-mGFP.catalase-peroxidase-T_{penDE}, $AmdS^+$	This study
DsRed-SKL GFP-chDEH	DsRed-SKL with integrated P_{gpdA}-mGFP.*chDEH*-T_{penDE}, $AmdS^+$	This study

proteins (18, 19). However, the molecular function of the peroxisomal Lon protease is not yet clear.

In this work we demonstrate that peroxisomal Lon is a multifunctional protein that acts as a protease, selectively degrading aberrant peroxisomal matrix proteins, but also assists in refolding of these components. As such, Lon is the first peroxisomal chaperone identified in fungi so far.

EXPERIMENTAL PROCEDURES

Strains and Growth Conditions—Penicillium chrysogenum strains used in this study are listed in Table 1. Cells were grown at 25 °C on mineral medium plates (20) supplemented with 1% glucose, 1% ethanol, or 1% oleic acid or in batch cultures on YGG medium (21), penicillin (PEN)[4] production medium supplemented with 0.05% phenylacetic acid (22), or in mineral medium containing 0.1% oleic acid and 0.05% Tween 80. To induce conidiospore formation, R-agar was used (21). Acetamide-resistant ($AmdS^+$) transformants were selected on plates containing 0.1% acetamide (23).

To determine fungal autolysis, *P. chrysogenum* strains were cultivated for 120 h in PEN media. Subsequently, each culture was divided into two halves, and 0.1% oleic acid and 0.05% Tween 80 were added to one-half. After incubation for 24 h, fungal biomass was determined as described previously (21). *Escherichia coli* DH5α was used for cloning purposes. *E. coli* Rosetta 2 cells (Novagen) were used for production of heterologous protein. *E. coli* cells were grown at 37 °C on LB medium supplemented with the appropriate antibiotics.

Molecular Techniques—Plasmids and oligonucleotides used in this study are listed in Tables 2 and 3. Standard DNA manipulations were performed according to established procedures (24). Transformation of *P. chrysogenum* protoplasts was performed as described previously (23). All PCR fragments were sequenced (Service XS). Restriction enzymes (Fermentas), T4 DNA ligase (Fermentas), and other DNA-modifying enzymes were used as recommended by the suppliers. PCR was carried out using high fidelity Phusion (Fermentas) polymerase. Southern blotting was performed according to the DIG High Prime labeling and detection kit (Roche Applied Science). *In silico* analysis of DNA sequences and construction of vector maps was carried out using Clone Manager 5 software (Scientific and Educational Software, Durham, NC).

Construction of the P. chrysogenum Pln Deletion Strain—The *pln* deletion cassette was constructed using the Multisite Gateway cloning system. The upstream (1.759 bp) and downstream (1.474 bp) flanking regions of *pln* gene were amplified by PCR with the primers AKR0007.PlnB4 and AKR0008.PlnB1 and with AKR0009.PlnB2 and AKR0010.PlnB3, respectively, using DS54465 genomic DNA as template. The resulting PCR products were introduced into pDONRP2R-P3 (3′-flanking region) and pDONRP4-P1R (5′-flanking region of *pln*) by using the Gateway BP clonase reaction, resulting in plasmids pENTR2.3-PLNdownstream and pENTR4.1-PLNupstream, respectively. Next, a Gateway LR reaction was performed using pENTR4.1-PLNupstream, pENTR221/PniadAMDS, pENTR2.3-PLN-downstream, and the destination vector pDEST R4-R3, resulting in the formation of the *pln* deletion construct pDest43_ΔPcPLN. This plasmid was linearized with AatII and transformed into *P. chrysogenum* DS54465 GFP-SKL protoplasts. Transformants were selected based on their ability to grow on acetamide as a sole nitrogen source. Disruption of the *pln* gene was confirmed by Southern blotting.

Construction of P. chrysogenum Strains Producing Various GFP Fusion Proteins—A plasmid enabling production of the Pln protein fused N-terminally with GFP was constructed using Multisite Gateway technology. The Pln coding sequence with a stop codon was amplified by PCR using primers AKR0005.PlnB1 and AKR0006.PlnB2 and a cDNA library as template (25). The obtained PCR product was cloned into the entry vector pDONR221, resulting in pENTR221_PcPLN. Subsequently, plasmids pENTR41/P_{pcbC}GFP, pENTR221_PcPLN, pENTR23-His8.T_{penDE}, and pDEST R4-R3/AMDS were recombined, resulting in a plasmid designated pDest43.pIPNS.eGFP.pcPLN.Tat. This plasmid was linearized with *Acc*65I and transformed to a *P. chrysogenum* strain producing DsRed-SKL.

A plasmid enabling production of a catalase-peroxidase protein fused N-terminally with GFP was constructed using the Multisite Gateway technology. The P*gpda* region was cut out from vector pBBK-007 and cloned into pGBRH2-mGFP in the place of P*pcbC* using *Asp*718I and BamHI, resulting in vector LMOP-Pgpda-mGFP. Next, the Pgpda-mGFP region was amplified by PCR using primers LMOp080 and LMOp081 and LMOP-Pgpda-mGFP as a template and recombined to pDONR4-1 in a BP recombination reaction, resulting in vector LMOP41-Pgpda-mGFP. The catalase-peroxidase coding sequence with a stop codon was amplified by PCR using primers KatGfor and KatGrev and cDNA library as template (25). The obtained PCR product was cloned into the entry vector pDONR221, resulting in pDONR221KatG. Subsequently, plasmids LMOP41pgpdAmGFP, pDONR221KatG, pENTR23-His8.T_{penDE}, and pDEST R4-R3/AMDS were recombined, resulting in a plasmid pGFPKatG. This plasmid was linearized

[4] The abbreviations used are: PEN, penicillin production; MBP, maltose-binding protein; TEV, tobacco etch virus; TBARS, thiobarbituric acid-reacting substance; SLS, static light scattering; DLS, dynamic light scattering; SAXS, small-angle x-ray scattering; MM, molecular mass; DHE, dihydroethidium; PTS1, peroxisomal targeting signal 1; CS, citrate synthase; s, scattering vector.

TABLE 2
Plasmids used in this study

Name	Description	Source/Reference
pDONR P4-P1R	Multisite Gateway vector, Kan^R Cm^R	Invitrogen
pDEST R4-R3	Multisite Gateway vector, Amp^R Cm^R	Invitrogen
pDONR 221	Multisite Gateway vector, Kan^R Cm^R	Invitrogen
pDONR P2R-P3	Multisite Gateway vector, Kan^R Cm^R	Invitrogen
pENTR221/PniadAMDS	pDONR 221 vector with P_{gpdA}-*amdS* cassette flanked by *niaD* sequences, Kan^R	Gift from J. G. Nijland
pENTR2.3-PLNdownstream	pDONR P2R-P3 with 3′-flanking region of *pln*, Kan^R	This study
pENTR4.1-PLNupstream	pDONR P4-P1R with 5′-flanking region of *pln*, Kan^R	This study
pDest43_ΔPcPLN	pDEST R4-R3 with *pln* deletion cassette, Amp^R	This study
pENTR221_PcPLN	pDONR 221 with *pln* CDS with stop codon, Kan^R	This study
pENTR41/P_{pcbC}GFP	pDONR P4-P1R with *pcbC* promoter and *eGFP* gene lacking a stop codon, Kan^R	(26)
pENTR23-His8.T_{penDE}	His-tag with C-terminal terminator of *penDE* gene, Kan^R	(59)
pDEST R4-R3/AMDS	pDESTR4-R3 with P_{gpdA}-*amdS* cassette, Amp^R	(26)
pDest43.pIPNS.eGFP.pcPLN.Tat	Expression vector with P_{pcbC}-*eGFP.pln*-T_{penDE} cassette, Amp^R	This study
LMOP41pgpdAmGFP	pDONR P4-P1R with *gpdA* promoter and *mGFP* gene lacking a stop codon, Kan^R	This study
pDONR221KatG	pDONR 221 with catalase-peroxidase CDS with stop codon, Kan^R	This study
pGFP.KatG	Expression vector with P_{gpdA}-*mGFP*-catalase-peroxidase-T_{penDE} cassette, Amp^R	This study
pBBK-007	Plasmid with P_{gpdA}-DsRed.SKL-T_{penDE} expression cassette, Amp^R	(50)
pGBRH2-mGFP	pBluescript vector with *pcbC* promoter, *mGFP* gene, and *penDE* terminator, Amp^R	(26)
LMOP-Pgpda-mGFP	pBluescript vector with *gpdA* promoter, *mGFP* gene, and *penDE* terminator, Amp^R	This study
pDONR221chDEH	pDONR 221 with oxidoreductase CDS with stop codon, Kan^R	This study
pGFP.chDEH	Expression vector with P_{gpdA}-*mGFP*.oxidoreductase-T_{penDE} cassette, Amp^R	This study
pMAL-c2	Expression vector for N-terminal MBP-tag fusions, Amp^R	New England Biolabs
pMDBPlnMBP	Expression vector containing *P. chrysogenum* Pln fused N-terminally to maltose-binding protein tag, Amp^R	This study
pMDBPlnHis	Expression vector containing *P. chrysogenum* Pln fused N-terminally to maltose-binding protein tag and C-terminally to the His tag, Amp^R	This study
pMDBLONTEV	Expression vector containing *P. chrysogenum* Pln fused N-terminally to maltose-binding protein tag and C-terminally to the His tag, with TEV protease cleavage site between MBP and Pln, Amp^R	This study
pMDBPlninMBP	Expression vector containing proteolytically inactive mutant of *P. chrysogenum* Pln, Pln^{in}, fused N-terminally to maltose-binding protein tag, Amp^R	This study
pMDBPlninHis	Expression vector containing proteolytically inactive mutant of *P. chrysogenum* Pln, Pln^{in}, fused N-terminally to maltose-binding protein tag and C-terminally to the His tag, Amp^R	This study
pMDBLONinTEV	Expression vector containing proteolytically inactive mutant of *P. chrysogenum* Pln, Pln^{in}, fused N-terminally to maltose-binding protein tag and C-terminally to the His tag, with TEV protease cleavage site between MBP and Pln^{in}, Amp^R	This study
pGEX-4T-2	Expression vector for N-terminal GST-tag fusions, Amp^R	GE Healthcare
pGSTKatG	Expression vector containing *P. chrysogenum* catalase-peroxidase fused N-terminally to glutathione *S*-transferase tag, Amp^R	This study

TABLE 3
Oligonucleotides used in this study

Name	Sequence (5′-3′)
AKR0007.PlnB4	GGGGACAACTTTGTATAGAAAAGTTGTGATATCTTGAACGGGGACG
AKR0008.PlnB1	GGGGACTGCTTTTTTGTACAAACTTGCAGGCCCTAGTGATGATGGAATGG
AKR0009.PlnB2	GGGGACAGCTTTCTTGTACAAAGTGGTCAGAGACGAGGCTGAAATCC
AKR0010.PlnB3	GGGGACAACTTTGTATAATAAAGTTGTATTGACTGGCATGAACGCATCAC
AKR0005.PlnB1	GGGGACAAGTTTGTACAAAAAAGCAGGCTTGATGGGAACAAACGGTAGAAGTACC
AKR0006.PlnB2	GGGGACCACTTTGTACAAGAAAGCTGGGTTCACAGTCGGCTCTCAACGAAG
KatGfor	GGGGACAAGTTTGTACAAAAAAGCAGGCTTTATGAGCGAATGTCCTGTTGCGC
KatGrev	GGGGACCACTTTGTACAAGAAAGCTGGGTTTCACAGGCGAGGACGACC
LMOp080	GGGGACAACTTTGTATAGAAAAGTTGTTACCGCGGCCGCTCTGTACAGTGAC
LMOp081	GGGGACTGCTTTTTTGTACAAACTTGCCTTGTACAGCTCGTCCATGCCGAG
chDEHfor	GGGGACAAGTTTGTACAAAAAAGCAGGCTTTATG GCCACCACGAACGAGTTC
chDEHrev	GGGGACCACTTTGTACAAGAAAGCTGGGTTTTACAGACGGGGCTGGTTGC
MDBPlnfor	ATAGGATCCATGGGAACAAACGGTAGAAGTACC
MDBPlnrev	AAACTGCAGTCACAGTCGGCTCTCAAC
MDBhisfor	CGTTGAGAGCCGACTGCATCACCATCACCATCACTGACTGCAGGCAAGC
MDBhisrev	GCTTGCCTGCAGTCAGTGATGGTGATGGTGATGCAGTCGGCTCTCAACG
MDB.TEV.for	GGATCGAGGGAAGGGAAAATCTTTACTTTCAAGGTATTTCAGAATTCGG
MDB.TEV.rev	CCGAATTCTGAAATACCTTGAAAGTAAAGATTTTCCCTTCCCTCGATCC
lonmutfor	CCCAAGGATGGTCCTGCTGCTGGTCTTGCCCACGCC
lonmutrev	GGCGTGGGCAAGACCAGCAGCAGGACCATCCTTGGG
GST.KatGfor	AAAGGATCCGAAAATCTTTACTTTCAAGGTATGAGCGAATGTCCTGTTGCGC
GST.KatGrev	AAAGAATTCTCACAGATCTTCTTCAGAAATAAGTTTTTGTTCCAGGCGAGGACGACCGGT

with NotI and transformed to a *P. chrysogenum* strain producing DsRed-SKL.

A plasmid enabling the production of the putative oxidoreductase protein fused N-terminally with GFP was constructed using Multisite Gateway technology. The putative oxidoreductase encoding sequence with a stop codon was amplified by PCR using primers chDEHfor and chDEHrev and a cDNA library as template (25). The obtained PCR product was cloned into the entry vector pDONR221, resulting in pDONR221chDEH. Subsequently, plasmids LMOP41pgpdAmGFP, pDONR221chDEH, pENTR23-His8.T_{penDE}, and pDEST R4-R3/AMDS were recombined, resulting in a plasmid pGFP-chDEH. This plasmid was linearized with AatII and transformed to *P. chrysogenum* producing DsRed-SKL. All transformants were

selected based on their ability to utilize acetamide as a sole nitrogen source.

Production and Purification of Pln—The coding sequence of Pln was amplified using a *P. chrysogenum* library as a template (25) and primers MDBPlnfor and MDBPlnrev containing BamHI and PstI sites, respectively. The obtained PCR product and expression vector pMAL-c2 (New England Biolabs) were digested with BamHI and PstI and ligated, resulting in plasmid pMDBPlnMBP, encoding *P. chrysogenum* Pln protein fused to maltose-binding protein (MBP) at the N terminus. Subsequently, a His_6 tag was introduced at the C terminus of the MBP-Pln fusion protein using the Lightening site-directed mutagenesis kit (Stratagene) and primers MDBhisfor and MDBhisrev and plasmid pMDBPlnMBP as a template, resulting in plasmid pMDBPlnHis. To introduce a tobacco etch virus (TEV) cleavage site between MBP and Pln, pMDBPlnHis plasmid, primers MDB.TEV.for, and MDB.TEV.rev and Lightening site-directed mutagenesis kit (Stratagene) were used, resulting in the final construct pMDBLONTEV. Correctness of the plasmid was confirmed by sequencing.

E. coli Rosetta 2 cells containing expression plasmid pMDBLONTEV were grown on LB medium at 37 °C to an optical density at 600 nm of 1.1 mM isopropyl 1-thio-β-D-galactopyranoside was added followed by 18 h incubation at 16 °C. Cells were harvested by centrifugation, and pellets were suspended in buffer A (50 mM Tris-HCl, 100 mM KCl, 10 mM $MgCl_2$, 5% glycerol, pH 8.0) and disrupted using a French press. The soluble fraction, which was obtained by centrifugation for 1 h at 16,000 × *g* at 4 °C was incubated with nickel-nitrilotriacetic acid resin (Qiagen) for 45 min at 4 °C. The resin was washed with buffer A containing 10 mM imidazole, and bound proteins were eluted with buffer A containing 300 mM imidazole. Fractions were analyzed by SDS-PAGE and Western blotting using α-His_6-tag antibodies (Santa Cruz Biotechnology). Fractions containing the MBP-Pln-His_6 fusion protein were pooled and loaded on amylose resin (New England Biolabs) equilibrated with buffer B (50 mM Tris-HCl, 100 mM KCl, 10 mM $MgCl_2$, 5% glycerol, pH 8.0) and incubated for 45 min at 4 °C. The resin was washed with buffer B, and bound Pln fusion protein was eluted with buffer B containing 10 mM maltose.

Generation and Purification of a Proteolytically Inactive Pln Mutant (Pln^{in})—The Pln mutant, S815A (Pln^{in}), encoded by plasmid pMDBPlninMBP, was generated using the pMDBPlnMBP plasmid, primers lonmutfor and lonmutrev, and the Lightening site-directed mutagenesis kit (Stratagene). To introduce a His_6 tag at the C terminus of the MBP-Pln^{in} fusion protein, plasmid pMDBPlninMBP used as the template, primers MDBhisfor and MDBhisrev and Lightening site-directed mutagenesis kit (Stratagene) were applied, resulting in plasmid pMDBPlninHis. To introduce a TEV cleavage site between MBP and Pln^{in}, the pMDBPlninHis plasmid was used as a template together with primers MDB.TEV.for and MDB.TEV.rev and the Lightening site-directed mutagenesis kit (Stratagene), resulting in the final construct pMDBLONinTEV. Correctness of the plasmid was confirmed by sequencing. pMDBLONinTEV plasmid was transformed into the Rosetta 2 *E. coli* cell strain. The Pln^{in} fusion protein was expressed and purified to homogeneity using the protocol for the Pln fusion protein.

Production and Purification of Catalase-Peroxidase—The coding sequence of catalase-peroxidase was amplified using *P. chrysogenum* cDNA library (25) as a template and primers GST.KatGfor and GST.KatGrev containing BamHI and EcoRI sites, respectively. The obtained PCR product and expression vector pGEX-4T-2 (GE Healthcare) were digested with BamHI and EcoRI and ligated, resulting in plasmid pGSTKatG, encoding catalase-peroxidase *P. chrysogenum* protein fused to glutathione *S*-transferase (GST) at the N terminus. Correctness of the plasmid was confirmed by sequencing.

E. coli Rosetta 2 cells containing expression plasmid pGSTKatG were grown on LB medium to an optical density at 600 nm of 1 and induced by the addition of 1 mM isopropyl 1-thio-β-D-galactopyranoside with simultaneous addition of 2.5 μM hemin (Sigma) followed with 18 h of incubation at 16 °C. Cells were harvested by centrifugation at 5200 × *g* for 10 min at 4 °C. The cell pellet was suspended in column buffer (50 mM NaH_2PO_4, 150 mM NaCl, 1 mM DTT, and 1 mM EDTA, pH 7.2) and disrupted using a French press. The soluble fraction, which was obtained by centrifugation for 1 h 16,000 × *g* at 4 °C, was incubated with glutathione Superflow resin (Qiagen) for 45 min at 4 °C. The resin was washed with column buffer, and bound proteins were eluted with elution buffer (50 mM Tris-HCl, 0.1 M NaCl, 50 mM reduced L-glutathione, 1 mM DTT, pH 8.0). Obtained fractions were analyzed by SDS-PAGE and Western blotting using α-c-Myc antibodies (Santa Cruz Biotechnology). Fractions containing GST-catalase-peroxidase were pooled and cleaved using AcTEV protease (Invitrogen). Separation of catalase-peroxidase from GST and TEV protease was accomplished using Superose 6 10/300 GL (GE Healthcare) column equilibrated with 50 mM NaH_2PO_4, 150 mM NaCl, pH 7.2. Purified GST-catalase-peroxidase was used for immunization of rabbits (Eurogentec, Seraing, Belgium; supplemental Fig. S5).

Biochemical Methods—Crude extract of *P. chrysogenum* cells were prepared as described previously (26). Protein concentrations were determined using the RC-DC assay system or Bio-Rad assay kit (Bio-Rad) using bovine serum albumin (BSA) as a standard. SDS-PAGE and Western blotting were carried out in accordance with established procedures. *P. chrysogenum* cell fractionation and peroxisome isolation were performed as described previously (26). Catalase activity was measured spectrophotometrically as described before (14). Peroxidase activity was determined spectrophotometrically as described by Fraaije *et al.* (27). Catalytic and peroxidatic activities were measured in *P. chrysogenum* extracts at the optimal pH values as determined for purified catalase-peroxidase (supplemental Fig. S4). The ATPase activity of Pln and Pln^{in} was measured colorimetrically using malachite green according to the instructions of the manufacturer (Innova Biosciences).

Isolation of Triton X-100-insoluble Peroxisomal Proteins—Triton X-100 insoluble proteins were isolated from fractions enriched in peroxisomes essentially as described previously (28). For identification of the proteins, bands of interest were cut from the SDS-PAGE gel and analyzed by mass spectrometry (MALDI-TOF peptide mass fingerprint and MALDI-TOF/TOF peptide sequencing, Alphalyse A/S, Denmark).

Analysis of Penicillin Production—β-Lactam antibiotic bioassays were performed as described previously (21). Quantita-

tive analysis of extracellular penicillin G was determined by HPLC using a Shim-Pack XR-ODS column (3.0-mm internal diameter × 75 mm) and an isocratic flow of 310 g·liter^{-1} acetonitrile, 640 mg·liter^{-1} KH_2PO_4, and 340 mg·liter^{-1} H_3PO_4. Peaks of penicillin G were detected at a wavelength of 254 nm.

Measurements of β-Oxidation of Fatty Acids in Intact Cells—Spores of *P. chrysogenum* strains were inoculated in YGG medium and incubated for 48 h. Next, cells were shifted to mineral medium supplemented with 0.1% oleic acid, 0.05% Tween 20 for 10 h. Subsequently, cells were washed and resuspended in phosphate-buffered saline (PBS). β-Oxidation activities were measured in intact cells as described previously (29). Cell suspensions were incubated in 200 μl of PBS containing 10 μM [1-^{14}C]stearate (C18:0). Reactions were allowed to proceed for 1 h at 28 °C followed by termination of the reactions by the addition of 50 μl of 2.6 M perchloric acid. Radiolabeled CO_2 was trapped overnight in 500 μl of 2 M NaOH. The ^{14}C-labeled β-oxidation products were subsequently collected after extracting the acidified material with chloroform/methanol/heptane and quantified in a liquid scintillation counter.

Lipid Peroxidation Analysis—Lipids peroxidation was quantified by determination of thiobarbituric acid-reacting substances (TBARSs) according to the method described by Paraszkiewicz *et al.* (30) using lysed protoplasts. The TBARS concentration was expressed as nmol of malondialdehyde/mg or protein.

In Vitro Protein Degradation Assays—Purified Pln and the proteolytically inactive mutant Pln^{in} were used for *in vitro* protease assays. Proteolytic activity against unfolded model proteins was assayed with α-casein (Sigma) or β-casein labeled with resorufin (Universal Protease Substrate, Roche Applied Science). For hydrolysis of α-casein, the assay buffer C consisting of 50 mM Tris-HCl, pH 8.0, 10 mM $MgCl_2$, 1 mM DTT with or without 4 mM ATP and the ATP regeneration system (50 mM creatine phosphate, 80 μg/ml creatine kinase) was used. Pln and the proteolytically inactive mutant (Pln^{in}) (final concentration of 0.26 μM) were incubated at 25 °C with 5.8 μM α-casein overnight. Proteolytic degradation of α-casein was detected using SDS-PAGE and Coomassie Brilliant Blue staining. For hydrolysis of β-casein labeled with resorufin Pln and Pln^{in}, 1.2 μM, were incubated at 25 °C with 0.1% of β-casein labeled with resorufin in buffer C according to the instructions of the manufacturer. Proteolysis was monitored spectrophotometrically at 574 nm.

The proteolytic activity against catalase-peroxidase was assayed in buffer C with or without 4 mM ATP and an ATP regeneration system (50 mM creatine phosphate, 80 μg/ml creatine kinase). Pln (0.46 μM) was incubated at 25 °C with native, thermally denatured or H_2O_2-treated catalase-peroxidase (0.52 μM). To prepare H_2O_2-treated catalase-peroxidase, catalase-peroxidase (final concentration 5.2 μM) was incubated with 5 mM H_2O_2 for 30 min at room temperature. Next H_2O_2 was removed by buffer exchange using an Amicon Ultra-4 and Microcon YM-3 centrifugation device (Millipore). To prepare thermally denatured catalase-peroxidase, catalase-peroxidase (at a concentration of 5.2 μM) was incubated for 10 min at 80 °C. Proteolytic activity was analyzed using SDS-PAGE electrophoresis and Coomassie Brilliant Blue staining. Quantification of catalase-peroxidase bands was performed with ImageJ software. The results from two independent experiments were averaged.

Catalase-Peroxidase Unfolding and Aggregation—Changes in intrinsic (tryptophan) fluorescence (excitation $\lambda = 295$ nm, emission $\lambda = 345$ nm) were measured at room temperature using 15 μM purified catalase-peroxidase in 50 mM Tris-HCl, pH 8.0, and 150 mM NaCl upon incubation for 10 min with different concentrations of hydrogen peroxide. Fluorescence measurements were performed using Fluoromax-3 spectrofluorometer (Jobin Yvon-Spex).

Aggregation of catalase-peroxidase (1.3 μM in 50 mM Tris-HCl, pH 8.0, and 150 mM NaCl) upon treatment with 20 mM hydrogen peroxide was monitored over a period of 60 min at room temperature by measuring light scattering at 360 nm in a PerkinElmer Life Sciences Lambda 35 spectrophotometer.

Citrate Synthase Aggregation and Refolding Assays—The capacity of Pln to prevent protein aggregation was determined using chemically denatured citrate synthase as a substrate as described previously (31). Citrate synthase (final concentration 30 μM of native enzyme; Sigma) was chemically denatured by incubation at room temperature in 6 M guanidinium/HCl and 20 mM DTT for at least 2 h. Aggregation was initiated by a 200-fold dilution of the denatured enzyme under vigorous stirring in 50 mM Tris-HCl, pH 8.0, with 5 mM $MgCl_2$ at 25 °C with or without Pln and with or without 1 mM ATP. The kinetic of citrate synthase aggregation was monitored by measuring the intensity of light scattering at 360 nm in a PerkinElmer Life Sciences Lambda 35 spectrophotometer.

To measure refolding activity of Pln, chemically denatured citrate synthase was prepared as described above at a concentration of 15 μM (31). Reactivation of citrate synthase was initiated by a 100-fold dilution of the denatured enzyme under vigorous stirring in 50 mM Tris-HCl, pH 8.0, with 5 mM $MgCl_2$ at 25 °C with or without Pln or Pln^{in} and with or without 1 mM ATP. The recovery of citrate synthase activity was tested as described (32) using oxaloacetic acid, acetyl-CoA, and dithiobis-[2-nitrobenzoic] acid (all from Sigma).

Static and Dynamic Light Scattering—Before static light scattering (SLS), dynamic light scattering (DLS), and small-angle x-ray scattering (SAXS) analysis, Pln^{in} was subjected to gel filtration using a Superdex S200 16/10 column equilibrated with 50 mM Tris, 150 mM NaCl, 1 mM DTT, 4 mM ATP, pH 8.0. The procedure used for SLS coupled to the ÄKTA system is described in Nettleship *et al.* (33). DLS measurements were performed on a DynaPro™ DLS (Protein solutions™) at 10 °C with the protein at a concentration of 1.1 μM.

SAXS Analysis—Synchrotron radiation x-ray scattering data from solutions of Pln^{in} were collected on the X33 camera of the EMBL on the storage ring DORIS III (DESY, Hamburg, Germany) (34). Using a photon counting Pilatus 1 M detector at a sample-detector distance of 2.7 m and a wavelength of $\lambda = 0.15$ nm, the range of momentum transfer $0.1 < s < 6$ nm^{-1} was covered ($s = 4\pi\sin\theta/\lambda$, where 2θ is the scattering angle). Four solute concentrations in the range 0.5–3.7 mg/ml were measured. To monitor radiation damage, 8 successive 15-s exposures were compared, and no significant changes were observed. The data were normalized to the intensity of the

transmitted beam and radially averaged; the scattering of the buffer was subtracted, and the difference curves were scaled for protein concentration. The low angle data collected from Pln^{in} were extrapolated to infinite dilution and merged with the higher concentration high angle data to yield the final composite scattering curve.

The forward scattering $I(0)$ and the radius of gyration R_g were evaluated using the Guinier approximation (35) assuming that at very small angles ($s < 1.3/R_g$) the intensity is represented as $I(s) = I(0)\exp(-(sR_g)2/3)$. These parameters were computed using the programs AUTORG and AUTOGNOM (36); the latter program also provided the pair distribution function of the particle $p(r)$ and the maximum dimension D_{max}. The molecular mass (MM) of Pln^{in} was evaluated by comparison of the forward scattering with that from a reference solution of bovine serum albumin (MM = 66 kDa).

Ab Initio Shape Determination—The "shape scattering" curve was further used to generate low resolution *ab initio* shapes of the Pln^{in} with the program DAMMIF (37). This program represents the particle shape with an assembly of densely packed beads and employs simulated annealing to construct a compact interconnected model fitting the experimental data $I_{exp}(s)$ to minimize discrepancy,

$$\chi^2 = \frac{1}{N-1}\sum_j \left[\frac{I_{exp}(s_j) - cI_{calc}(s_j)}{\sigma s_j}\right]^2 \qquad \text{(Eq. 1)}$$

where N is the number of experimental points, c is a scaling factor, and $I_{calc}(s)$ and $\sigma(s_j)$ are the calculated intensity and the experimental error at the momentum transfer s_j, respectively. Ten DAMMIF runs were performed to check the stability of solution, and the results were well superimposable with each other. These models were averaged to determine common structural features using the programs DAMAVER (38) and SUPCOMB (39). The latter program aligns two arbitrary low or high resolution models represented by ensembles of points by minimizing a dissimilarity measure called normalized spatial discrepancy. For every point (bead or atom) in the first model, the minimum value among the distances between this point and all points in the second model is found, and the same is done for the points in the second model. These distances are added and normalized against the average distances between the neighboring points for the two models. Generally, normalized spatial discrepancy values close to unity indicate that the two models are similar. The program DAMAVER generates the average model of the set of superimposed structures and also specifies the most typical model (*i.e.* that having the lowest average normalized spatial discrepancy with all the other models of the set).

Molecular Modeling—The program BUNCH (40) combines rigid body and *ab initio* modeling of proteins consisting of domains (for which high resolution models are available) linked by flexible loops of unknown structure. A simulated annealing protocol is employed to find the optimal positions and orientations of the domains moved as rigid bodies and probable conformations of the flexible linkers attached to the appropriate terminal residues of domains. These linkers are represented as interconnected chains of dummy residues (41), where protein fragments are substituted by a flexible chain of residues separated by 0.38 nm. The x-ray scattering intensity from the entire model is expressed as,

$$I(s) = 2\pi\sum_{l=0}^{\infty}\sum_{m=(-)l}^{l}\left[\sum_k A^{(k)}{}_{lm}(s) + \sum_i D^{(i)}{}_{lm}(s)\right]^2 \qquad \text{(Eq. 2)}$$

Here, $A^{(k)}{}_{lm}(s)^H$ are the partial scattering amplitudes of the rigid domains calculated from their atomic coordinates using CRYSOL (42). The partial scattering amplitudes of the linkers $D^{(i)}{}_{lm}(s)$ are computed from the positions of the dummy residues using the form factor equal to that of an average residue in water (41). Starting from an arbitrary configuration of domains and linkers, the program performs random modifications of the model maintaining the structures of the domains and connectivity of the linkers.

Microscopy—Confocal laser scanning microscopy images were obtained using a Zeiss LSM510 confocal laser scanning microscope equipped with a Zeiss Plan-Neofluar ×100/1.3 and Zeiss Plan-Apochromatic ×63/1.4 oil objectives. Images were acquired using AIM 4.2 software (Carl Zeiss). GFP fluorescence was analyzed by excitation of the cells with a 488-nm argon-krypton laser, and fluorescence was detected with BP 500–530 Photo Multiplier Tube. DsRed fluorescence was analyzed by excitation of the cells with a 543-nm argon/krypton laser, and fluorescence was detected with a BP 565–615 Photo Multiplier Tube.

Wide-field fluorescence microscopy was performed with a Zeiss Axio Observer Z1 fluorescence microscope. Images were obtained with an EC-Plan-Neofluar ×100/1.3 objective and coolsnap HQ2 Camera (Roper Scientific Inc.). The GFP signal was analyzed with a 470/40-nm bandpass excitation filter, a 495-nm dichromatic mirror, and a 525/50-nm bandpass emission filter. DsRed as well as dihydroethidium (DHE, Invitrogen) fluorescence was visualized with a 545/25-nm bandpass excitation filter, a 570-nm dichromatic mirror, and a 605/70-nm bandpass emission filter. Z-stack images were made with an interval of 1 μm. Images were acquired using AxioVision 4.7 software (Carl Zeiss). *P. chrysogenum* mycelia were stained with fluorescent probes before microscopy investigation in accordance with manuals provided by the suppliers (Invitrogen). Maximum fluorescence intensities of DHE-stained nuclei were measured using ImageJ software.

For electron microscopy *P. chrysogenum* cells were prepared as described previously (43). Image analysis was performed using ImageJ (rsbweb.nih.gov), and figures were prepared using Adobe Photoshop CS3.

RESULTS

P. chrysogenum Peroxisomes Contain a Protease of the Lon A Protein Family—Previously, we identified a putative peroxisomal Lon protease (designated Pln) in the fungus *P. chrysogenum* by *in silico* identification of proteins that contain a putative peroxisomal targeting signal 1 (PTS1 (26). We confirmed the peroxisomal localization of this protein by fluorescence microscopy using cells producing a GFP-Pln fusion protein in conjunction with DsRed-SKL as a peroxisomal matrix marker (Fig. 1*A*).

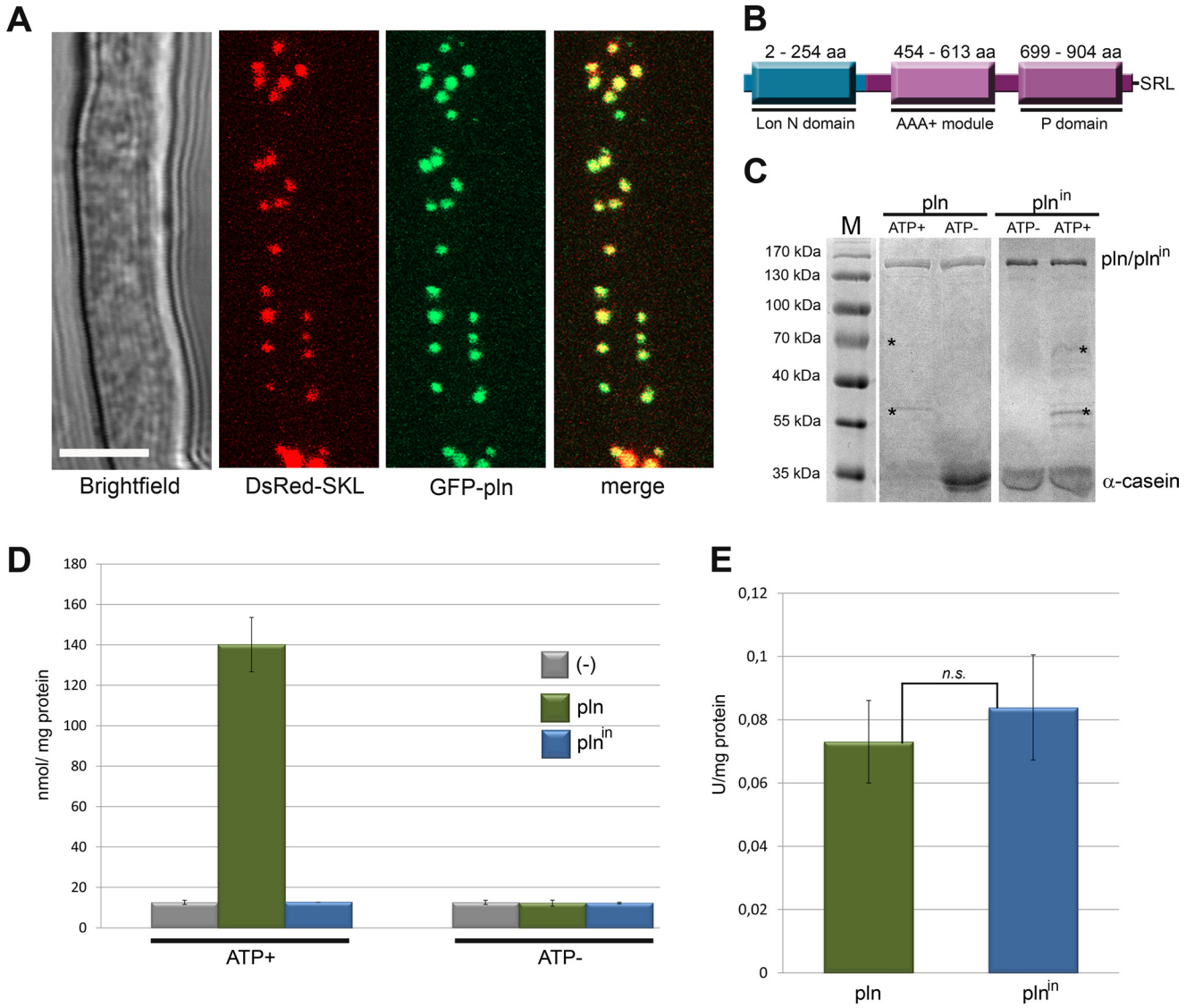

FIGURE 1. **Peroxisomes contain an ATP-dependent Lon protease.** *A*, shown is confocal laser scanning microscopy analysis of the subcellular localization of peroxisomal Lon protease using cells producing GFP-Pln and DsRed-SKL as marker of peroxisomes. GFP fluorescence co-localized with DsRed. Confocal laser scanning microscopy pictures were taken after 40 h of growth in PEN medium. The *scale bar* represents 5 μm. *B*, shown is a schematic representation of the domain architecture of *P. chrysogenum* Pln showing the three conserved domains as well as the C-terminal PTS1 tripeptide, SRL. *aa*, amino acids. *C*, *P. chrysogenum* Pln degrades α-casein in an ATP-dependent manner. Purified Pln or the inactive variant Pln^{in} was incubated with α-casein in the presence (*ATP*$^{+}$) or absence (*ATP*$^{-}$) of ATP and an ATP regeneration system. After overnight incubation, the samples were subjected to SDS-PAGE, and the gels were stained with Coomassie Brilliant Blue. Upon incubation in the presence of ATP and Pln, the bulk of the α-casein protein was degraded, as evident from the absence of the 35-kDa α-casein band. The bands marked with *asterisks* represent proteins of the ATP regeneration system. *D*, Pln degrades β-casein in an ATP-dependent manner. Quantitative analysis of the proteolytic degradation of resorufin-labeled β-casein by Pln (*green*) and Pln^{in} (*blue*) in the presence (*ATP*$^{+}$) or absence (*ATP*$^{-}$) of ATP and an ATP regeneration system is shown. Controls lacking Pln or Pln^{in} (−) are shown in *gray*. *E*, ATPase activities of purified Pln and Pln^{in}. *n.s.*, statistically not significant (Student's *t* test). *Error bars* in *D* and *E* represent S.D.

Inspection of the protein sequence revealed that Pln belongs to the Lon A protein family. These proteins have three functional domains: an N-terminal (Lon N domain), an ATPase (AAA+ module with Walker A and B motifs), and a protease domain (P domain with conserved catalytic dyad) (Fig. 1*B*).

Pln, purified to homogeneity as MBP fusion protein upon production in *E. coli* (supplemental Fig. S1), proved to be rather unstable in contrast to its proteolytically inactive variant (Pln^{in}; S815A, see below). However, both MBP fusion proteins (Pln and Pln^{in}) precipitated upon cleavage of MBP by TEV protease. We, therefore, performed all further *in vitro* studies using MBP fusion proteins. *In vitro* assays revealed that Pln displayed ATP-driven proteolytic activity toward α-casein and β-casein, both unfolded protein substrates (Fig. 1, *C* and *D*). As expected, this activity was fully abolished by the single amino acid substitution, S815A, in the conserved catalytic dyad. Also no proteolytic activity was detected when the assays were performed in the absence of ATP (Fig. 1, *C* and *D*). Purified Pln showed ATPase activity, which was not abolished by the mutation in the catalytic dyad (Fig. 1*E*).

P. chrysogenum Pln Is a Heptameric Protein—Previous reports indicate that Lon proteases form large oligomeric complexes, ranging from tetramers to octamers (44–46). To gain insight into the oligomeric state of *P. chrysogenum* Pln, we subjected the MBP-Pln^{in} fusion protein to SLS, DLS, and SAXS in

the presence of ATP (Table 4, supplemental Fig. S2). SLS and DLS analysis suggested that Pln^{in} consists of 6.7 and 7.2 monomers, respectively, indicative of a heptamer (Table 4). Such an oligomeric state has also been reported for mitochondrial Lon from *Saccharomyces cerevisiae* (47).

Next, we performed SAXS analysis of Pln^{in} to obtain a low resolution model of the protein (supplemental Fig. S2). The molecular mass of the protein estimated from the forward scattering amounted to 1100 ± 100 kDa comparable to the SLS and DLS estimates of 980 ± 110 and 1060 ± 330 kDa respectively. The experimental radius of gyration R_g and maximum size D_{max} (10.3 ± 9 and 34 ± 3 nm, respectively) point to an oblate structure. The smaller angles (up to $s = 0.5\ nm^{-1}$) can be fitted ($\chi = 2.5$) with an oblate ellipsoid of revolution with a diameter of 29 nm and a height 9.4 nm. Assuming that one Pln^{in} monomer is 147 kDa, the oligomeric state of Pln^{in} in solution could be hexameric, heptameric, or octameric. The low resolution shape of Pln^{in} was first reconstructed *ab initio* using the bead modeling program DAMMIF (37) employing the range of scattering vectors up to $s = 0.8\ nm^{-1}$. Ten *ab initio* models were constructed using the symmetries P6, P7, and P8 (hexameric, heptameric, and octameric, respectively) and compared; the reconstructions in P6 and P7 were more reliable (normalized spatial discrepancy = 0.82 ± 0.08 and 0.75 ± 0.09, respectively) than in P8 (normalized spatial discrepancy = 2.13 ± 0.25). Using the available crystal structure of MBP (PBD code 1ANF; Ref. 48) as well as two models built with the program SWISS-Model (49) corresponding to amino acids 11–201 and 378–902 in Pln^{in} (no structure of full-length Lon is available), hexamers, heptamers, and octamers were constructed using the program BUNCH (40). P8 models exhibited many domain clashes, effectively ruling out an octameric state for Pln^{in}. The P6 models had a systematically worse fit ($\chi = 1.4$) compared with the P7 models ($\chi = 1.2$), although the difference is not large. However this coupled with the SLS and DLS data inclines us to favor a heptameric state for Pln^{in} in solution. This assumption is supported by our fit to the ellipsoid, as the obtained height also corresponds to a P7 model. A putative P6 model would require a 1.8× bigger height. The most probable *ab initio* P7 model out of 10 reconstructions (Fig. 2) displays an oblate, ring-shaped, and seven-armed structure. The BUNCH rigid body model, which is comparable with the DAMMIF model in overall appearance, is similar to the transmission electron microscopy model of mitochondrial Lon (47).

TABLE 4
SLS, DLS, and SAXS data

Static light scattering	Molecular weight (M_r)	984 kDa (± 11%)
	Number weighted mean (Mn)	982 kDa (± 11%)
	Poly-disparity (M_r/Mn)	1.0 (± 16%)
Dynamic light scattering	Hydrodynamic radius	11.5 nm (± 31%)
	Molecular weight	1060 kDa (± 31%)
SAXS analysis	Radius of gyration	10.3 nm (± 9%)
	Molecular weight	1100 kDa (± 10%)
Theoretical molecular weight of Pln^{in}		147 kDa (monomer)
		882 kDa (hexamer)
		1029 kDa (heptamer)
		1176 kDa (octamer)

Lon Deficiency Is Associated with a Defect in Growth on Oleic Acid and Enhanced Oxidative Stress—To gain insight into the *in vivo* function of Pln, a *P. chrysogenum* knock-out strain was constructed (designated *pln*). The *P. chrysogenum pln* strain displayed normal growth on complex media (R-agar) as well as on mineral media containing glucose or ethanol as sole carbon source (Fig. 3*A*). The cells also grew normally on PEN media (data not shown), which was accompanied by the production of penicillin G levels that were similar to the parental strain (Fig. 3, *D* and *E*).

Remarkably, *pln* cells displayed a severe defect in growth on oleic acid as a sole carbon source (Fig. 3*A*). Further analysis

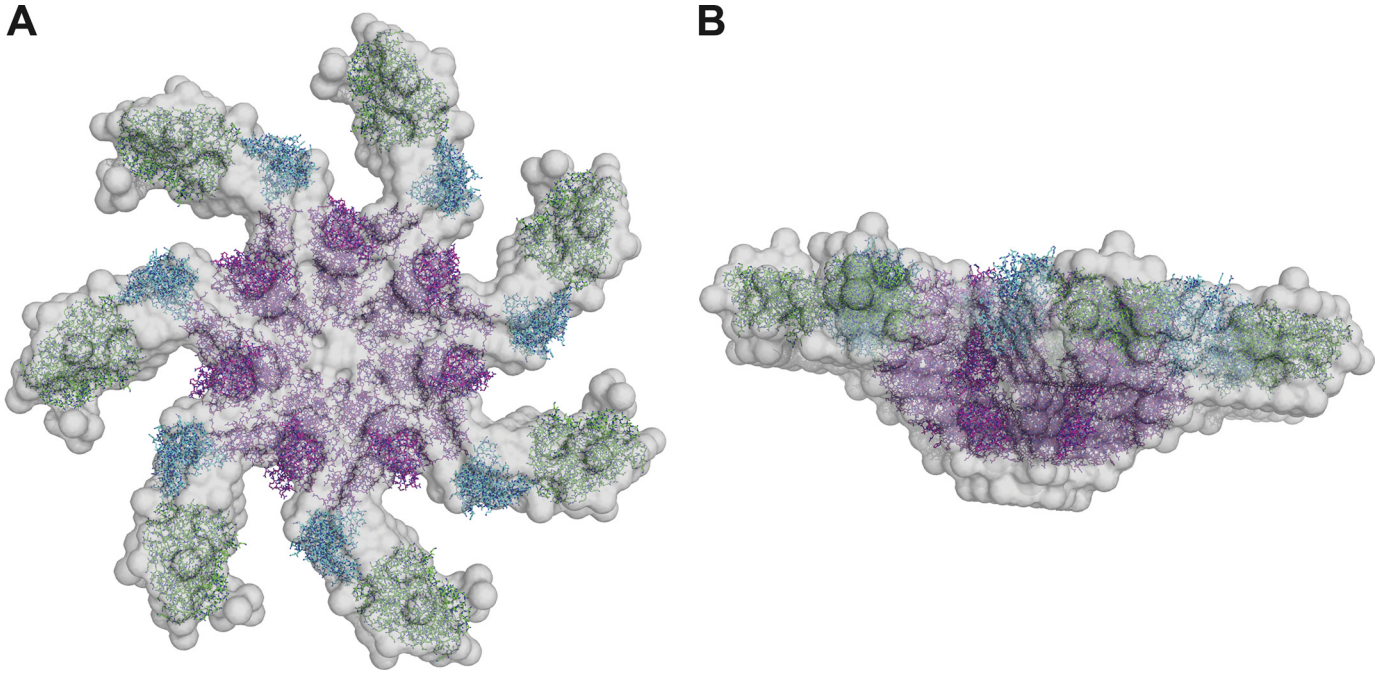

FIGURE 2. ***Ab initio* models of heptameric MBP-Pln^{in}.** The DAMMIF bead model is shown in *gray*. The BUNCH rigid body model, consisting of the crystal structure of MBP (*green*) and the homology models of residues 11–201 (*cyan*) and 378–902 (*magenta*), is shown in stick representation. *A*, top view. *B*, side view.

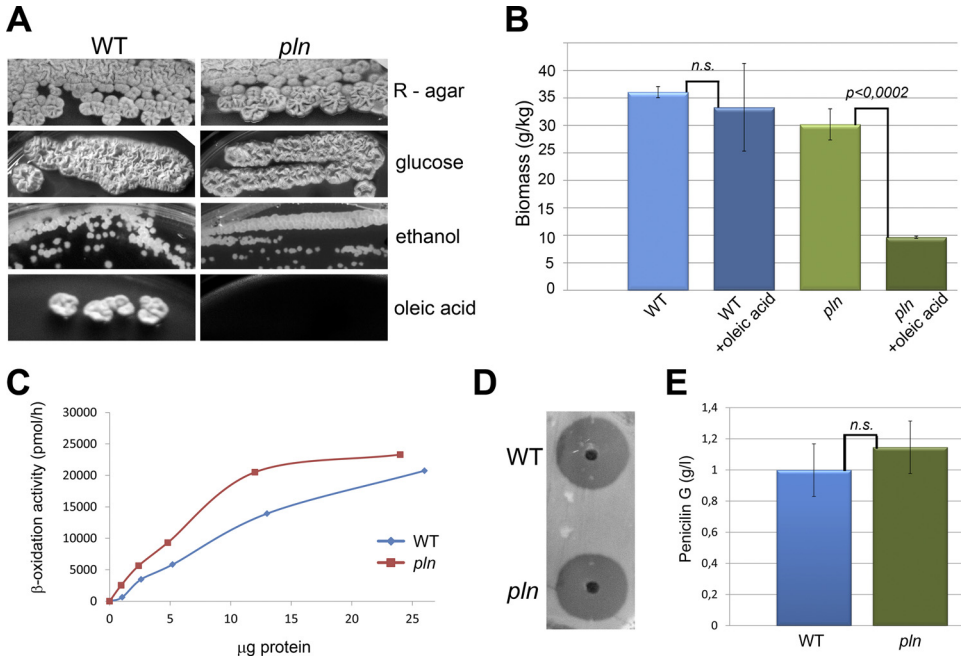

FIGURE 3. **Growth properties and penicillin production.** *A*, growth of *pln* and wild-type (*WT*) cells on agar plates containing complex medium (*R-agar*) or mineral medium supplemented with 1% glucose, 1% ethanol, or 1% oleic acid as sole carbon sources is shown. Plates were incubated at 25 °C for 5–10 days. *B*, shown is quantification of biomass 24 h after the addition of 0.1% oleic acid to WT or *pln* cultures grown for 120 h on PEN medium. *Error bars* represent S.D. *C*, shown is fatty acid (C18:0) β-oxidation in intact cells of WT (*blue*) and *pln* (*red*) incubated for 10 h in medium containing 0.1% oleate. β-Oxidation is expressed as the sum of [^{14}C]CO_2 and water-soluble β-oxidation products produced/µg of protein used in the assay. *D*, spent media of *pln* and WT strains cultivated on penicillin G production media for 5 days were diluted and loaded into wells of a bioassay plate overgrown with cells of a *Micrococcus luteus* strain. Cell densities of the wild-type and *pln* cultures (in terms of dry weight/liter) were comparable. After 24 h of incubation at 30 °C, the sizes of the growth inhibition zones were similar, indicating that similar concentrations of penicillin G were produced. *E*, spent medium of *pln* and wild-type cultures grown for 5 days on PEN medium were used to quantitatively determine penicillin G levels by HPLC. Average values from three independent cultures are presented for each strain. The *bars* represent S.D. *n.s.* , statistically not significant (Student's *t* test).

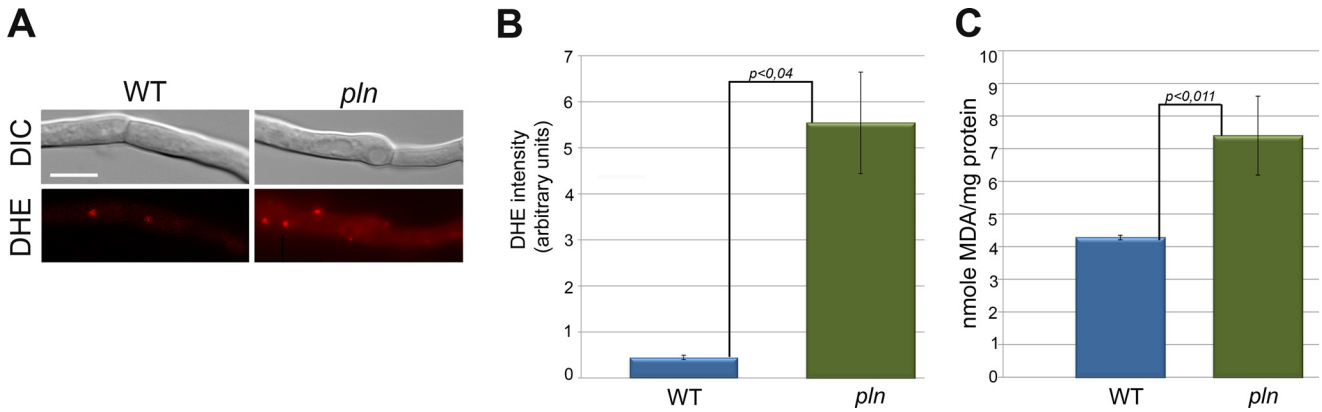

FIGURE 4. **Lack of peroxisomal Lon protease results in enhanced oxidative stress.** *A*, shown are fluorescence microscopy images of DHE stained WT and *pln* cells grown for 120 h in PEN medium after the addition of 0.1% oleic acid and further incubation for 12 h. *pln* cells show enhanced DHE fluorescence relative to the wild-type control. The *scale bars* represent 5 µm. *DIC*, differential interference contrast. *B*, shown is quantification of DHE fluorescence intensities from cells shown in *A*. *Error bars* represent S.E. *C*, lipid peroxidation was quantified by determination of TBARSs. Measurements were performed using cell homogenates of wild-type and *pln* cells grown for 120 h on PEN medium. The TBARS concentration is expressed as nmol of malondialdehyde (*MDA*)/mg of protein. *Error bars* represent S.D. Statistical analysis was performed with Student's *t* test.

suggested that oleic acid was toxic for *pln* cells. This was indicated by the observation that the addition of oleic acid to stationary phase cultures of *pln* cells resulted in a decrease in biomass (Fig. 3*B*). The oleic acid growth defect was not due to a block in peroxisomal fatty acid metabolism as C18:0 β-oxidation was not decreased in these cells (Fig. 3*C*).

Deletion of *PLN* in *Hansenula polymorpha* resulted in enhanced oxidative stress (14). We, therefore, also analyzed whether the lack of Pln influences the homeostasis of reactive oxygen species in *P. chrysogenum*. Cells were stained with DHE, a fluorescent dye that specifically reacts with intracellular $O_2^{\cdot-}$ and is converted to the red fluorescent compound ethidium, which irreversibly binds to double-stranded DNA and appears as punctate nuclear staining (Fig. 4*A*). Enhanced nuclear staining with DHE was observed in *pln* cells grown on PEN medium relative to the wild-type control (supplemental Fig S3). This difference was much more pronounced when peroxisome proliferation and the peroxisomal β-oxidation pathway were induced by the addition of oleic acid (50); Fig. 4, *A* and *B*).

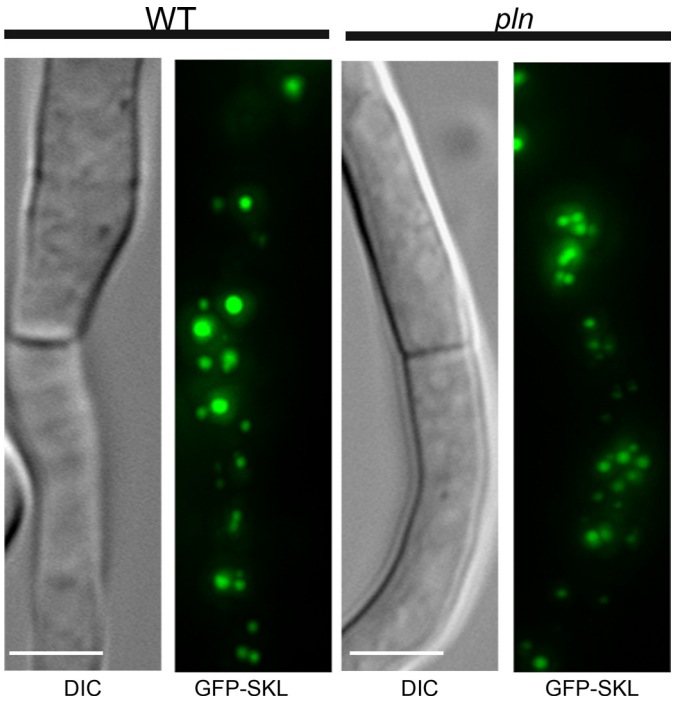

FIGURE 5. **Localization of GFP containing a PTS1 in WT and *pln* cells.** Fluorescence microscopy images showing GFP-SKL localization in WT and *pln* cells grown for 120 h in PEN media. Like in the wild-type control, no cytosolic GFP was observed in *pln* cells. The *scale bars* represent 5 μm. *DIC*, differential interference contrast.

We also measured the difference in lipid oxidative damage in *pln* and wild-type cells, which is determined by the measurement of TBARSs. Malondialdehyde is an important byproduct of lipid peroxidation and reacts with thiobarbituric acid. As shown in Fig. 4*C*, significantly enhanced lipid peroxidation was observed in *pln* cells grown on PEN media relative to that observed in the wild-type control.

The Absence of Pln Results in the Formation of Protein Aggregates in the Peroxisomal Matrix—Cells of the *pln* strain showed normal import of peroxisomal matrix proteins, as was evident from the peroxisomal localization of GFP-SKL in *pln* cells, which was similar to that in the wild-type control (Fig. 5). The absence of Pln was associated with the accumulation of protein aggregates in the peroxisomal matrix that were visualized as electron-dense inclusions in the organelle lumen by electron microscopy (Fig. 6*B*). These inclusions were confined to peroxisomes and never observed in other cell compartments of cells of the *pln* strain. Also, peroxisomal protein aggregates were never observed in wild-type control cells (Fig. 6*A*). The protein content of the aggregates that are present in *P. chrysogenum pln* cells likely represents substrates of Pln. To identify these proteins, the aggregates (defined as proteins that are not solubilized by Triton X-100) were isolated from Triton X-100-treated peroxisomal fractions by high velocity centrifugation. SDS-PAGE revealed two distinct protein bands that were enhanced in the insoluble fractions obtained from organelles isolated from *pln* cells relative to identical fractions obtained from wild-type controls (Fig. 6*C*). Mass spectrometry revealed that these bands consisted of a putative catalase-peroxidase and a putative oxidoreductase from the glucose-methanol-choline (*GMC*) oxidoreductase family (Fig. 6*C*). Hex1, which forms a crystalline inclusion of Woronin bodies, is not solubilized by Triton X-100 (51), and was observed in both the insoluble fractions isolated from *pln* and wild-type control organelles. The peroxisomal localization of catalase-peroxidase and glucose-methanol-choline oxidoreductase was confirmed using *P. chrysogenum* cells producing N-terminal GFP fusions of these proteins and DsRed-SKL as peroxisomal marker (Fig. 6, *D* and *E*).

Unfolded Catalase-Peroxidase Is a Substrate of Pln in Vitro—Catalase-peroxidase, one of the major Triton X-100 insoluble proteins in peroxisome fractions of *pln* cells (Fig. 6*C*), was selected for further analysis. As peroxisomes are oxidative organelles, we studied whether oxidative stress may cause catalase-peroxidase enzyme inactivation or protein aggregation.

Catalase-peroxidase was produced in *E. coli* and purified to homogeneity (supplemental Fig. S1). Enzyme assays revealed that the catalase-peroxidase enzyme displayed catalase and peroxidase activities with pH optima of 6–7 and 5, respectively (supplemental Fig. S4). Treatment of purified catalase-peroxidase protein with increasing concentrations of H_2O_2 resulted in a decrease in intrinsic Trp fluorescence and peroxidase enzyme activity, indicative for protein unfolding (Fig. 7*A*). Relatively low concentrations of H_2O_2 already caused significant changes in Trp fluorescence and peroxidase activity (enzyme activity decreased by 40% after treatment with 100 μM H_2O_2). Catalase-peroxidase was also prone to aggregation upon treatment with H_2O_2 *in vitro*, as evident from light scattering measurements (Fig. 7*B*). Finally, we tested whether catalase-peroxidase was a substrate for Pln using an *in vitro* degradation assay. These studies revealed that the native protein was not degraded by Pln. However, upon pretreatment with H_2O_2 or preincubation at high temperature, the protein was degraded by Pln (Fig. 7, *C* and *D*). These data indicate that unfolded catalase-peroxidase, but not the native protein, is a substrate of the peroxisomal Lon.

Pln Displays Chaperone-like Activity—The presence of aggregates in peroxisomes of *pln* cells could be explained by aggregation of unfolded catalase-peroxidase protein. Western blot analysis revealed that *pln* cells contained enhanced catalase-peroxidase protein levels (Fig. 7*E*), whereas enzyme activity measurements revealed that the catalytic (Fig. 7*F*) and peroxidatic activities (Fig. 7*G*) were reduced. These observations suggest that Pln may display, additional to its proteolytic activity, also chaperone activity *in vivo*. To test the putative chaperone activity of Pln, citrate synthase (CS) was used as a substrate in *in vitro* protein refolding experiments. To test if purified Pln can suppress aggregation of this substrate, guanidine hydrochloride-denatured CS was diluted into buffer containing purified Pln. Relative to the control without Pln, a significant decrease in CS aggregation (~40%) was observed (Fig. 8*A*). This decrease was independent of the presence of ATP (Fig. 8, *A* and *B*). The addition of BSA instead of Pln did not prevent CS aggregation (Fig. 8*C*). Aggregation of denatured CS was inhibited by Pln in a dose-dependent manner (Fig. 8*D*) and was the most efficient at a ratio of one or more Pln monomers to two CS monomers. Purified Pln also stimulated reactivation of chemically denatured CS (Fig. 8*F*), which was also optimal at a ratio of at least 1:2 Pln monomers to CS monomers (Fig. 8*E*). This stimulatory effect of Pln was not observed in the absence of ATP (Fig. 8*G*). Interestingly, the proteolytically inactive mutant of

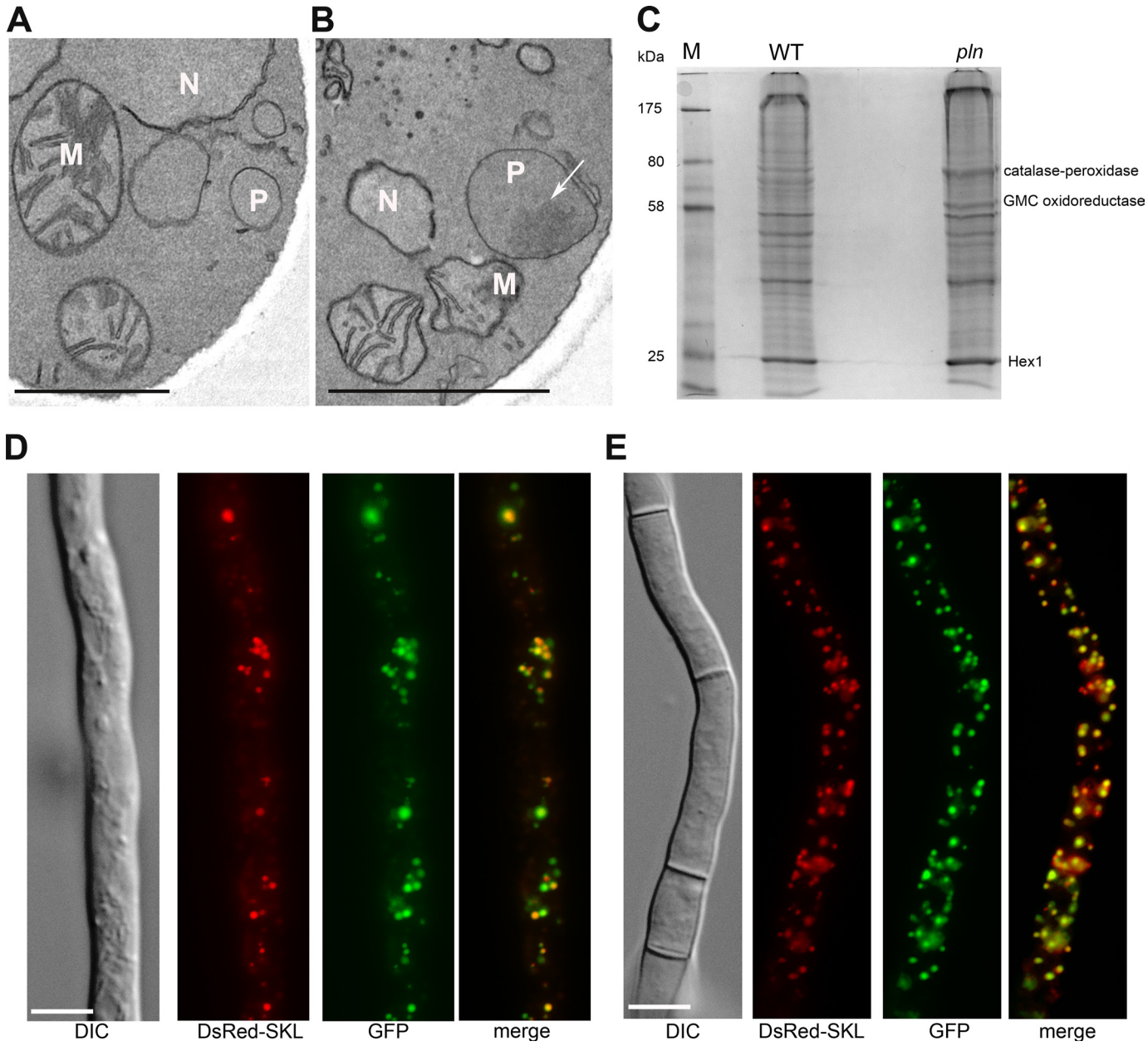

FIGURE 6. **The absence of Pln results in the formation of protein aggregates in the peroxisomal matrix.** *A* and *B*, electron microscopy images of a detail of a wild-type (*A*) and *pln* (*B*) cell show the presence of a protein aggregate (*arrow*, Fig. 6*B*) in the peroxisomal matrix of the *pln* cell. The cells were fixed with $KMnO_4$. *P*, peroxisome; *M*, mitochondrion; *N*, nucleus. The *scale bar* represents 1 μm. *C*, shown is a Coomassie Brilliant Blue (*CBB*)-stained SDS-PAGE gel of Triton-X100-insoluble proteins isolated from peroxisomal fractions obtained from wild-type and *pln* cells. The indicated protein bands were identified by mass spectrometry. *GMC*, glucose-methanol-choline. *D* and *E*, shown are subcellular localizations of N-terminal GFP fusion proteins of catalase-peroxidase (*D*) and glucose-methanol-choline oxidoreductase (*E*), analyzed by fluorescence microscopy in cells cultivated for 40 h in PEN media. DsRed-SKL was used as a marker of peroxisomes. The *scale bar* represents 5 μm.

Pln (Pln^{in}) facilitated refolding of CS with the same efficiency as the active protein (Fig. 8*F*). These data suggest that Pln is a multifunctional enzyme that, besides proteolytic activity, displays chaperone-like activity that is independent of the proteolytic catalytic dyad.

DISCUSSION

In this work we provide evidence that peroxisomes of the fungus *P. chrysogenum* contain an isoform of the Lon protease, termed Pln, a member of the AAA protein family, that displays a dual function as ATP-stimulated protease in conjunction with a role as molecular chaperone. As such, Pln is the first chaperone that is identified in fungal peroxisomes.

Because proteins are marginally stable macromolecules with a limited lifespan, we imagined that also peroxisomal matrix proteins require constant housekeeping processes. As yet, the fate of luminal proteins within the oxidative milieu of peroxisomes was, however, still an enigma. Recently, a Lon protease was identified in the peroxisomal matrix of rat (15), yeast (14), and plant (52). Studies performed in *H. polymorpha* indeed suggest that the deletion of peroxisomal Lon protease (*pln*) affected organelle quality

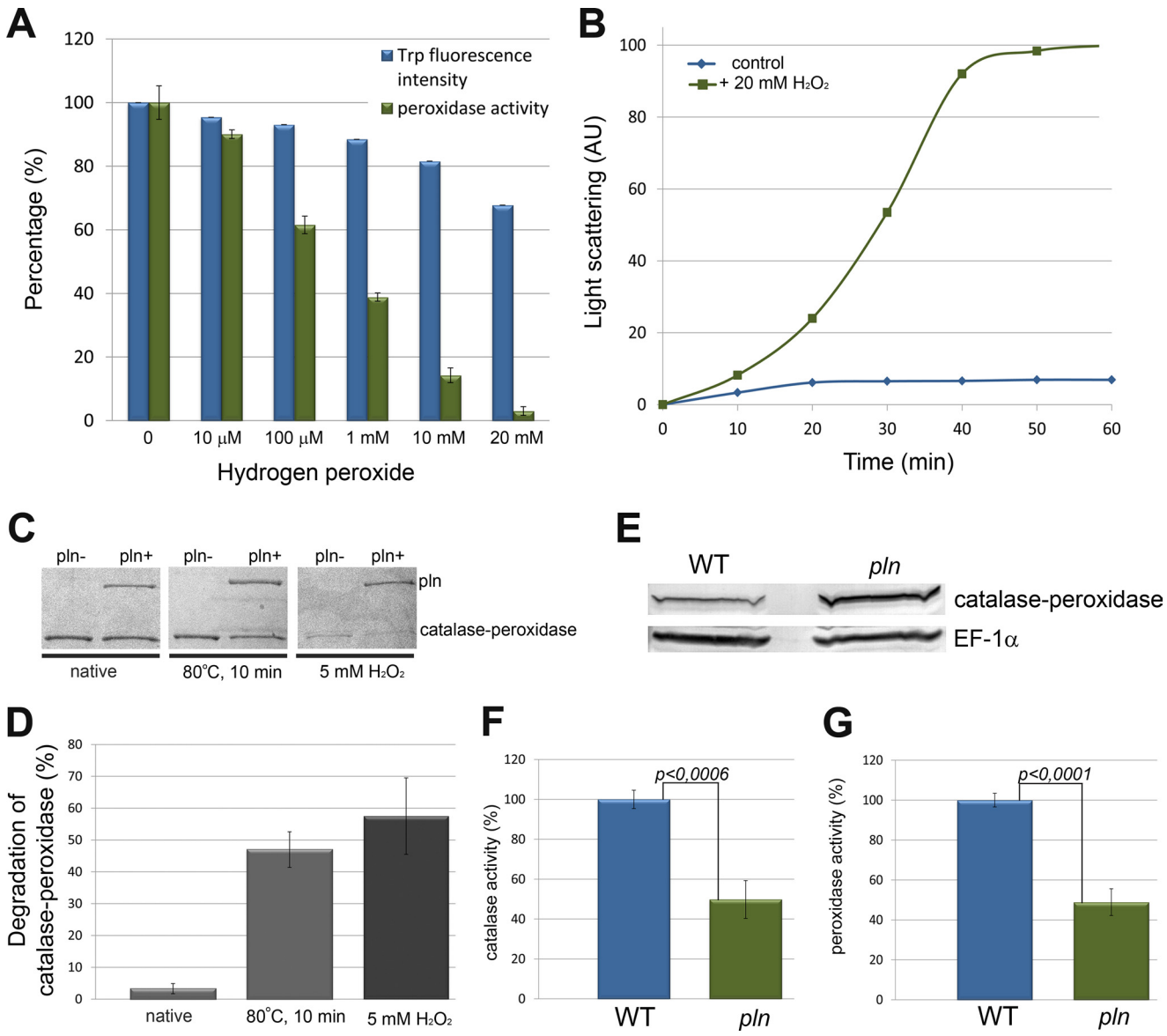

FIGURE 7. **Damaged catalase-peroxidase is the substrate of Pln.** *A*, catalase-peroxidase unfolds (*blue*) and loses peroxidase activity (*green*) upon hydrogen peroxide treatment. Unfolding of catalase-peroxidase (15 μM) was monitored by measurement of changes in intrinsic tryptophan fluorescence. The protein was incubated for 10 min with the indicated concentrations of hydrogen peroxide before the measurements. Values are expressed as percentages of signal/activity. *Error bars* represent S.E. *B*, catalase-peroxidase is prone to aggregation upon hydrogen peroxide treatment as analyzed by light scattering measurements at 360 nm. *AU*, absorbance units. *C*, Coomassie Brilliant Blue-stained gel demonstrates that H_2O_2 or heat-treated catalase-peroxidase is a substrate for Pln *in vitro*. The amount of catalase-peroxidase protein treated with H_2O_2 or an elevated temperature, but not untreated (native) protein, decreased upon incubation with Pln relative to the control without Pln. Representative gels are presented. *D*, quantification of the catalase-peroxidase bands (compare Fig. 7*C*) from two independent degradation experiments revealed a 57.5% ($\pm$12%) decrease in the level of catalase-peroxidase protein treated with H_2O_2 and a 47% ($\pm$5.6) reduction of catalase-peroxidase protein levels when exposed to elevated temperature (80 °C) relative to the control sample without Pln (set to 100%). In contrast, no significant degradation of the untreated, native catalase-peroxidase protein was detected (decrease of 3.3 $\pm$ 1.6%). *E*, a Western blot shows the catalase-peroxidase protein levels in cell extracts of wild-type and *pln* cells grown for 120 h on PEN medium. Quantification of the bands revealed an ~2-fold increase in catalase-peroxidase protein in *pln* cells. Equal protein amounts were loaded per lane. EF-1α was used as loading control. The experiment was performed twice, and a representative blot is presented. The blots were prepared from the same samples as used for enzyme activity measurements (shown in Fig. 7, *F* and *G*). Catalase (*F*) and peroxidase (*G*) activities in cell extracts of wild-type and *pln* cells grown for 120 h on PEN medium are shown. Values are expressed as the percentage of the specific enzymatic activity of wild type. The observed differences in enzyme activities between wild-type and *pln* cells are statistically significant (Student's *t* test). *Error bars* represents S.E.

control and had detrimental effects on peroxisome function and cell vitality (14).

The lack of the peroxisomal Lon protease in *P. chrysogenum* was associated with the accumulation of protein aggregates in the peroxisomal matrix, suggesting that Pln is required to prevent accumulation of misfolded proteins and their subsequent aggregation in the organelle matrix. It is tempting to speculate that aggregate-forming proteins in *pln* cells represent the preferred substrates of Pln. As major constituents of the aggregates, we identified a heme-containing catalase-peroxidase and a putative FAD-dependent oxidoreductase from the glucose-methanol-choline family. The catalase-peroxidase protein was the major component of the aggregate and was, therefore, analyzed further. Interestingly, our data indicate that purified catalase-peroxidase is prone to oxidative damage and loses activity and forms aggregates upon exposure to hydrogen peroxide.

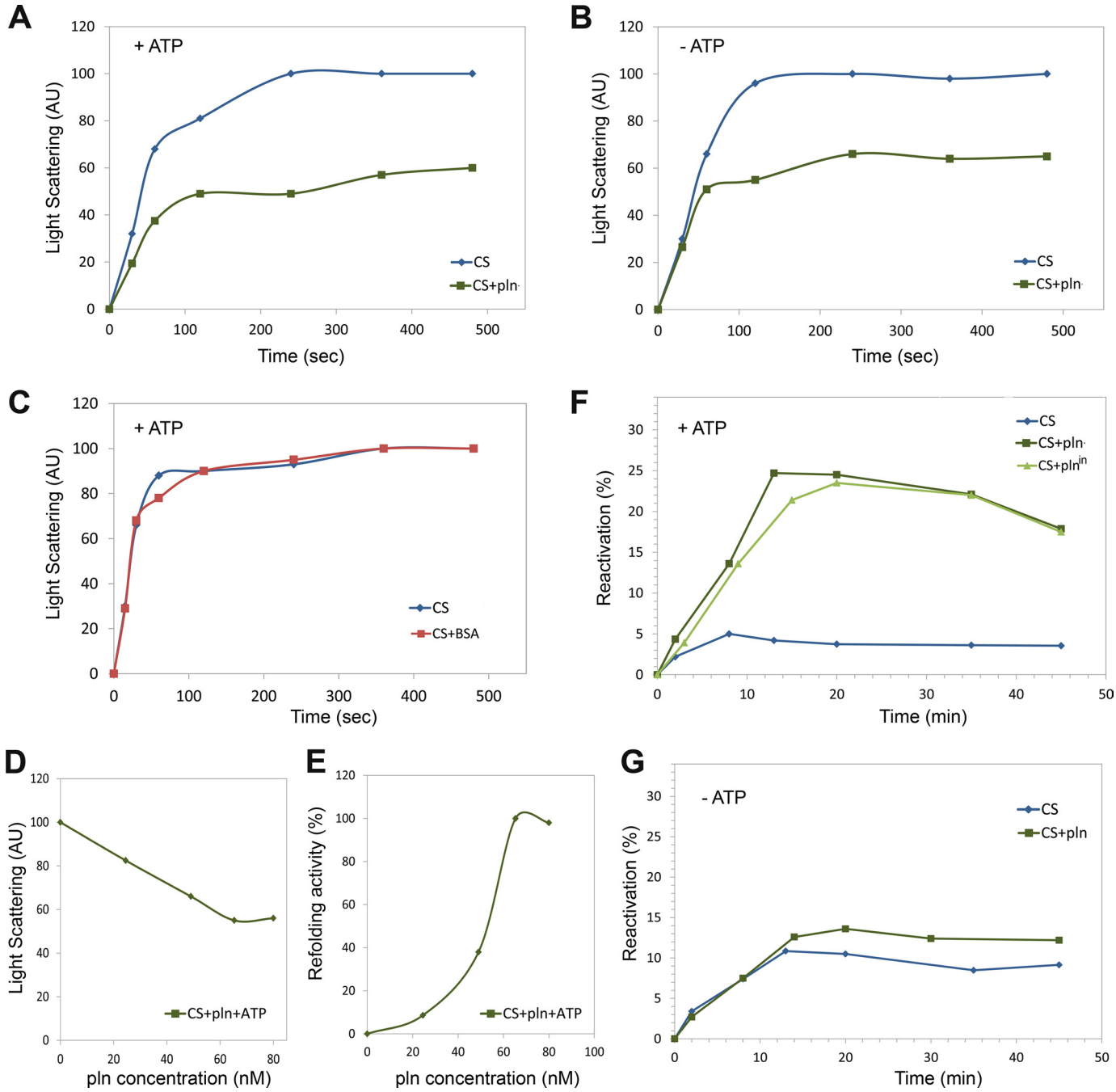

FIGURE 8. **Peroxisomal Lon protease displays chaperone-like activity.** *A* and *B*, the aggregation kinetics of 150 nM denatured CS were monitored in the absence of Pln or presence of 80 nM Pln in the presence (*A*) or absence (*B*) of 1 mM ATP. *AU*, absorbance units. *C*, a reduction in aggregation was not observed when the reaction was performed in the presence of 80 nM BSA and ATP (*red*). *D*, denatured CS was diluted to a final concentration 150 nM in a solution supplemented with different concentrations of Pln (monomer). Aggregation kinetics of CS were measured. Normalized light scattering values obtained after 360 s are shown. The highest measured value was set to 100. *E*, reactivation of 150 nM denatured CS was determined in the presence of 1 mM ATP and different concentrations of Pln (monomer). CS reactivation was determined after 15 min of incubation. The highest refolding activity of Pln was set to 100%. *F*, reactivation of 150 nM denatured CS was determined in the presence of 1 mM ATP. Without the addition of Pln, only minor reactivation was observed. However, in the presence of 80 nM Pln or Pln^{in}, ~25% of the CS was reactivated. *G*, reactivation of denatured CS (150 nM) was similar in reactions containing Pln or lacking Pln when the reactions were performed in the absence of ATP.

Western blot analysis revealed that catalase-peroxidase protein levels were elevated in crude extracts of *pln* cells relative to wild type. This indicates that catalase-peroxidase most likely constitutes a substrate of the Pln protease *in vivo*. Indeed, damaged catalase-peroxidase (heat denaturated or H_2O_2 treated), but not the native enzyme, was degraded *in vitro* by Pln *in vitro*. *pln* cells also showed reduced catalase-peroxidase enzyme activities. Together with our *in vitro* experiments, which indicate that Pln has chaperone activity, this observation suggests that Pln also shows chaperone activity toward catalase-peroxidase. Hence, the increased catalase-peroxidase protein levels together with the reduced enzyme activities most likely is the result of the absence of both the proteolytic and chaperone activities of the Lon protease in *P. chrysogenum pln* cells.

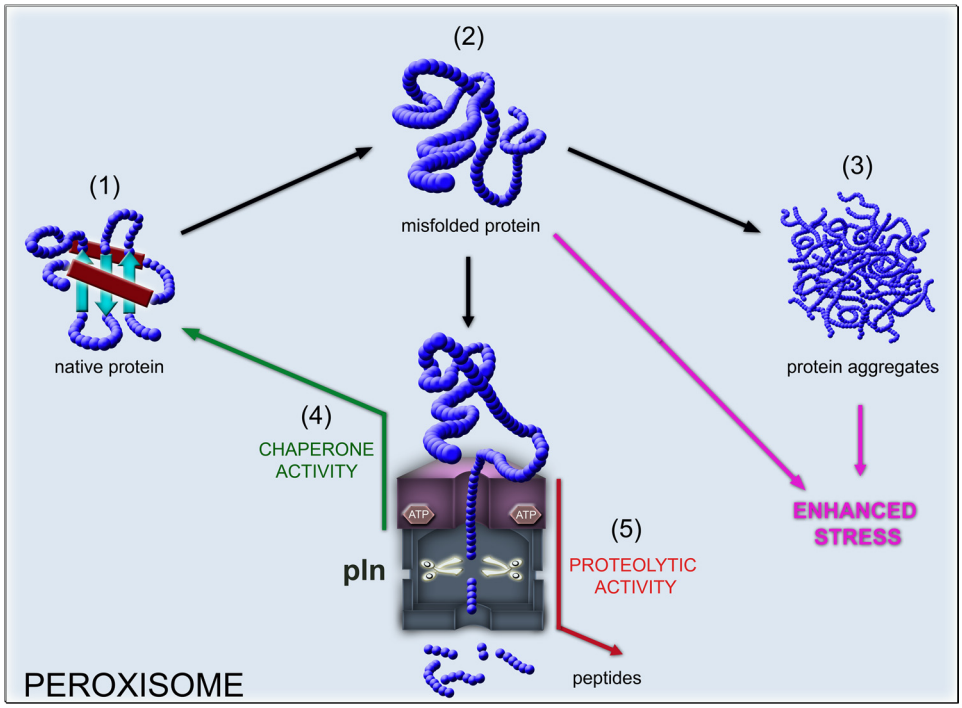

FIGURE 9. **Model proposing the role of Pln in protein quality control in the peroxisome matrix.** Peroxisomal matrix proteins most likely are delivered to the organelle in a folded conformation (*1*). Peroxisomal matrix proteins encounter stress (*e.g.* oxidative stress generated by peroxisomal metabolism) that may accelerate protein damage (*2*) that can be followed by protein aggregation (*3*). To cope with this, peroxisomes possess a bifunctional ATP-dependent Pln that controls the quality of peroxisomal proteome in two ways, as a chaperone protein (*4*) that facilitates refolding of destabilized peroxisomal proteins and as a protease that digests misfolded macromolecules (*5*) to prevent their aggregation. The lack of Pln may lead to accumulation of damaged proteins that may compromise peroxisomal function and cell viability.

As yet the bulk of the research on Lon substrate specificity has been carried out using bacterial Pln homologues and artificial substrates. Although some possible substrates have been proposed for mitochondrial Lon in man and bakers' yeast, direct evidence for Lon substrates has not been presented so far (19). Here, we show for the first time a *bona fide* substrate for Lon protease, namely catalase-peroxidase for Pln from *P. chrysogenum.* Our data are consistent with the view that catalase peroxidase, which is a crucial component of peroxisomal antioxidant defense system (26), may exemplify a particularly vulnerable peroxisomal protein and, therefore, requires substantial turnover by peroxisomal Lon protease.

In *Arabidopsis thaliana*, peroxisomal Lon protease was proposed to be involved in sustaining matrix protein import into peroxisomes of older cotyledon (52). For mammalian systems, contradictory results were reported; in cells of a HeLa cell line, peroxisomal matrix import was not affected by knockdown of peroxisomal Lon protease (53), whereas overproduction of a dominant negative variant of this protein in HEK293 cells resulted in mislocalization of the PTS1-containing enzyme catalase (54). In the filamentous fungus *P. chrysogenum* as well as in the methylotropic yeast *H. polymorpha*, peroxisomal Lon protease is not involved in sustaining matrix protein import, as mislocalization of GFP-SKL was not observed in these organisms (this study and Ref. 14).

Surprisingly, in *P. chrysogenum*, various peroxisomal metabolic pathways function normally in the absence of Pln except for the utilization of oleate, a process that requires peroxisomal β-oxidation. Moreover, oleic acid also was shown to be toxic to the cells. Activity measurements of the β-oxidation pathway revealed no major change in *pln* cells relative to wild-type controls. Hence, oleic acid oxidation can proceed normally in these cells. However, strongly enhanced oxidative stress was observed upon the addition of oleic acid to *pln* cells. A possible explanation for the failure of the cells to grow on oleate is that enhanced levels of H_2O_2, produced in the first oxidation step of oleate, inactivates the catalase-peroxidase protein, thereby releasing its co-factor heme, resulting in the generation of oxygen radicals via iron from heme in the Fenton reaction and thus leading to cell death.

Our biophysical data suggest that the *P. chrysogenum* peroxisomal Lon protease forms heptameric ring-shaped assemblies. Almost all members of the AAA protein family assemble into ring-like higher order structures (55). A stoichiometry of seven subunits was previously reported for mitochondrial Lon from *S. cerevisiae* (47), whereas bacterial Lon proteases are hexameric (19). Stahlberg *et al.* (47) demonstrated that significant conformational changes occur in yeast mitochondrial Lon protease depending on the presence of ATP. Because we analyzed Pln only in the presence of ATP, we cannot exclude that peroxisomal Lon protease undergoes similar ATP-dependent structural changes.

The hallmark of the AAA family of proteins is the ATP binding domain (AAA module), which contains conserved Walker A and B motifs, that function as an unfoldase (56). Cycles of ATP binding and hydrolysis drive conformational changes, creating pulses of pulling force that denature the substrate and translocate the unfolded polypeptide through the pore into the proteolytic chamber. Several cycles of protein binding and release are required to accomplish protein degradation by

ATP-fueled proteolytic machines (57). Our *in vitro* experiments indicate that Pln displays ATP-driven refolding activities. Our data suggest that a destabilized protein that is captured by the peroxisomal Lon is able to escape from translocation into the proteolytic chamber and, instead of being degraded, is refolded. This is noteworthy as the observed chaperone activity was independent of the proteolytic activity of Pln. In agreement with these findings, a chaperone-like activity has been suggested before for the mitochondrial isoform of Lon protease (58) based on *in vivo* experiments.

Taken together, our data suggest that the *P. chrysogenum* peroxisomal Lon is a multifunctional protein (Fig. 9) and represents the first fungal peroxisomal chaperone identified. Our data are consistent with the view that Pln represents the first example of a conserved peroxisomal protein that functions in peroxisome matrix quality control and actively assists in refolding of peroxisomal matrix proteins.

Acknowledgments—We gratefully acknowledge Dr. F. Ulrich Hartl for valuable discussions. We thank Stefan Weber, Katarzyna Łukaszuk, and Annemarie Kralt for assistance in various parts of this study, EMBL Hamburg for providing resources, and the SPC facility (EMBL Hamburg) for technical support.

REFERENCES

1. Dobson, C. M. (2003) Protein folding and misfolding. *Nature* **426,** 884–890
2. Jaenicke, R. (1998) Protein self-organization *in vitro* and *in vivo*: partitioning between physical biochemistry and cell biology. *Biol. Chem.* **379,** 237–243
3. Jahn, T. R., and Radford, S. E. (2005) The Yin and Yang of protein folding. *FEBS J.* **272,** 5962–5970
4. Ellis, R. J., and Minton, A. P. (2006) Protein aggregation in crowded environments. *Biol. Chem.* **387,** 485–497
5. Hartl, F. U., Bracher, A., and Hayer-Hartl, M. (2011) Molecular chaperones in protein folding and proteostasis. *Nature* **475,** 324–332
6. Tyedmers, J., Mogk, A., and Bukau, B. (2010) Cellular strategies for controlling protein aggregation. *Nat. Rev. Mol. Cell Biol.* **11,** 777–788
7. Powers, E. T., Morimoto, R. I., Dillin, A., Kelly, J. W., and Balch, W. E. (2009) Biological and chemical approaches to diseases of proteostasis deficiency. *Annu. Rev. Biochem.* **78,** 959–991
8. Islinger, M., Grille, S., Fahimi, H. D., and Schrader, M. (2012) The peroxisome. An update on mysteries. *Histochem. Cell Biol.* **137,** 547–574
9. Wanders, R. J., and Waterham, H. R. (2006) Peroxisomal disorders. The single peroxisomal enzyme deficiencies. *Biochim. Biophys. Acta* **1763,** 1707–1720
10. Steinberg, S. J., Raymond, G. V., Braverman, N. E., and Moser, A. B. (1993) *Peroxisome Biogenesis Disorders, Zellweger Syndrome Spectrum*, University of Washington, Seattle, WA
11. Antonenkov, V. D., Grunau, S., Ohlmeier, S., and Hiltunen, J. K. (2010) Peroxisomes are oxidative organelles. *Antioxid. Redox Signal.* **13,** 525–537
12. Reeder, B. J., Svistunenko, D. A., Cooper, C. E., and Wilson, M. T. (2004) The radical and redox chemistry of myoglobin and hemoglobin. From *in vitro* studies to human pathology. *Antioxid. Redox Signal* **6,** 954–966
13. Walton, P. A., Hill, P. E., and Subramani, S. (1995) Import of stably folded proteins into peroxisomes. *Mol. Biol. Cell* **6,** 675–683
14. Aksam, E. B., Koek, A., Kiel, J. A., Jourdan, S., Veenhuis, M., and van der Klei, I. J. (2007) A peroxisomal lon protease and peroxisome degradation by autophagy play key roles in vitality of *Hansenula polymorpha* cells. *Autophagy* **3,** 96–105
15. Kikuchi, M., Hatano, N., Yokota, S., Shimozawa, N., Imanaka, T., and Taniguchi, H. (2004) Proteomic analysis of rat liver peroxisome. Presence of peroxisome-specific isozyme of Lon protease. *J. Biol. Chem.* **279,** 421–428
16. Wagner, I., Arlt, H., van Dyck, L., Langer, T., and Neupert, W. (1994) Molecular chaperones cooperate with PIM1 protease in the degradation of misfolded proteins in mitochondria. *EMBO J.* **13,** 5135–5145
17. von Janowsky, B., Knapp, K., Major, T., Krayl, M., Guiard, B., and Voos, W. (2005) Structural properties of substrate proteins determine their proteolysis by the mitochondrial AAA+ protease Pim1. *Biol. Chem.* **386,** 1307–1317
18. Bota, D. A., and Davies, K. J. (2002) Lon protease preferentially degrades oxidized mitochondrial aconitase by an ATP-stimulated mechanism. *Nat. Cell Biol.* **4,** 674–680
19. Venkatesh, S., Lee, J., Singh, K., Lee, I., and Suzuki, C. K. (2012) Multitasking in the mitochondrion by the ATP-dependent Lon protease. *Biochim. Biophys. Acta* **1823,** 56–66
20. van Dijken, J. P., Otto, R., and Harder, W. (1976) Growth of *Hansenula polymorpha* in a methanol-limited chemostat. Physiological responses due to the involvement of methanol oxidase as a key enzyme in methanol metabolism. *Arch. Microbiol.* **111,** 137–144
21. Bartoszewska, M., Kiel, J. A., Bovenberg, R. A., Veenhuis, M., and van der Klei, I. J. (2011) Autophagy deficiency promotes β-lactam production in. *Penicillium chrysogenum*. *Appl. Environ. Microbiol.* **77,** 1413–1422
22. Hillenga, D. J., Versantvoort, H. J., Driessen, A. J., and Konings, W. N. (1994) Structural and functional properties of plasma membranes from the filamentous fungus. *Penicillium chrysogenum*. *Eur. J. Biochem.* **224,** 581–587
23. Opaliński, L., Kiel, J. A., Homan, T. G., Veenhuis, M., and van der Klei, I. J. (2010) *Penicillium chrysogenum* Pex14/17p. A novel component of the peroxisomal membrane that is important for penicillin production. *FEBS J.* **277,** 3203–3218
24. Sambrook, J., Fritsch, E. F., Maniatis, T., and Ford, N. (1989) *Molecular Cloning: A Laboratory Manual,* 2nd Ed., Cold Spring Harbor Laboratory Press, Cold Spring Harbor, NY
25. Kiel, J. A., Hilbrands, R. E., Bovenberg, R. A., and Veenhuis, M. (2000) Isolation of *Penicillium chrysogenum PEX1* and *PEX6* encoding AAA proteins involved in peroxisome biogenesis. *Appl. Microbiol. Biotechnol.* **54,** 238–242
26. Kiel, J. A., van den Berg, M. A., Fusetti, F., Poolman, B., Bovenberg, R. A., Veenhuis, M., and van der Klei, I. J. (2009) Matching the proteome to the genome. The microbody of penicillin-producing *Penicillium chrysogenum* cells. *Funct. Integr. Genomics* **9,** 167–184
27. Fraaije, M. W., Roubroeks, H. P., Hagen, W. R., and Van Berkel, W. J. (1996) Purification and characterization of an intracellular catalase-peroxidase from. *Penicillium simplicissimum*. *Eur. J. Biochem.* **235,** 192–198
28. Bender, T., Lewrenz, I., Franken, S., Baitzel, C., and Voos, W. (2011) Mitochondrial enzymes are protected from stress-induced aggregation by mitochondrial chaperones and the Pim1/LON protease. *Mol. Biol. Cell* **22,** 541–554
29. van Roermund, C. W., Elgersma, Y., Singh, N., Wanders, R. J., and Tabak, H. F. (1995) The membrane of peroxisomes in *Saccharomyces cerevisiae* is impermeable to NAD(H) and acetyl-CoA under *in vivo* conditions. *EMBO J.* **14,** 3480–3486
30. Paraszkiewicz, K., Bernat, P., Naliwajski, M., and Długoński, J. (2010) Lipid peroxidation in the fungus *Curvularia lunata* exposed to nickel. *Arch. Microbiol.* **192,** 135–141
31. Buchner, J., Grallert, H., and Jakob, U. (1998) Analysis of chaperone function using citrate synthase as nonnative substrate protein. *Methods Enzymol.* **290,** 323–338
32. West, S. M., Kelly, S. M., and Price, N. C. (1990) The unfolding and attempted refolding of citrate synthase from pig heart. *Biochim. Biophys. Acta* **1037,** 332–336
33. Nettleship, J. E., Brown, J., Groves, M. R., and Geerlof, A. (2008) Methods for protein characterization by mass spectrometry, thermal shift (ThermoFluor) assay, and multiangle or static light scattering. *Methods Mol. Biol.* **426,** 299–318
34. Roessle, M., Klaering, R., Ristau, U., Robrahn, B., Jahn, D., Gehrmann, T., Konarev, P., Round, A., Fiedler, S., Hermes, C., and Svergun, D. (2007) Upgrade of the small-angle X-ray scattering beamline X33 at the European Molecular Biology Laboratory, Hamburg. *J. Appl. Crystallogr.* **40,** 190–194

35. Guinier, A. (1939) La diffraction des rayons X aux tres petits angles; application a l'etude de phenomenes ultramicroscopiques. *Ann. Phys.* (*Paris*) **12,** 161–237
36. Petoukhov, M. V., Konarev, P., Kikhney, A. G., and Svergun, D. I. (2007) *ATSAS* 2.1. Toward automated and web-supported small-angle scattering data analysis. *J. Appl. Crystallogr.* **40,** 223–228
37. Franke, D., and Svergun, D. I. (2009) DAMMIF, a program for rapid *ab initio* shape determination in small-angle scattering. *J. Appl. Crystallogr.* **42,** 342–346
38. Volkov, V. V., and Svergun, D. I. (2003) Uniqueness of *ab initio* shape determination in small-angle scattering. *J. Appl. Crystallogr.* **36,** 860–864
39. Kozin, M., and Svergun, D. I. (2001) Automated matching of high and low resolution structural models. *J. Appl. Crystallogr.* **34,** 33–41
40. Petoukhov, M. V., and Svergun, D. I. (2005) Global rigid body modeling of macromolecular complexes against small-angle scattering data. *Biophys. J.* **89,** 1237–1250
41. Petoukhov, M. V., Eady, N. A., Brown, K. A., and Svergun, D. I. (2002) Addition of missing loops and domains to protein models by x-ray solution scattering. *Biophys. J.* **83,** 3113–3125
42. Svergun, D. I., Barberato, C., and Koch, M. H. J. (1995) CRYSOL. A program to evaluate x-ray solution scattering of biological macromolecules from atomic coordinates. *J. Appl. Crystallogr.* **28,** 768–773
43. Waterham, H. R., Titorenko, V. I., Haima, P., Cregg, J. M., Harder, W., and Veenhuis, M. (1994) The *Hansenula polymorpha* PER1 gene is essential for peroxisome biogenesis and encodes a peroxisomal matrix protein with both carboxyl- and amino-terminal targeting signals. *J. Cell Biol.* **127,** 737–749
44. Goldberg, A. L., Moerschell, R. P., Chung, C. H., and Maurizi, M. R. (1994) ATP-dependent protease La (lon) from *Escherichia coli*. *Methods Enzymol.* **244,** 350–375
45. Roudiak, S. G., Seth, A., Knipfer, N., and Shrader, T. E. (1998) The lon protease from *Mycobacterium smegmatis*. Molecular cloning, sequence analysis, functional expression, and enzymatic characterization. *Biochemistry* **37,** 377–386
46. Lee, A. Y., Hsu, C. H., and Wu, S. H. (2004) Functional domains of *Brevibacillus thermoruber* lon protease for oligomerization and DNA binding. Role of N-terminal and sensor and substrate discrimination domains. *J. Biol. Chem.* **279,** 34903–34912
47. Stahlberg, H., Kutejová, E., Suda, K., Wolpensinger, B., Lustig, A., Schatz, G., Engel, A., and Suzuki, C. K. (1999) Mitochondrial Lon of *Saccharomyces cerevisiae* is a ring-shaped protease with seven flexible subunits. *Proc. Natl. Acad. Sci. U.S.A.* **96,** 6787–6790
48. Quiocho, F. A., Spurlino, J. C., and Rodseth, L. E. (1997) Extensive features of tight oligosaccharide binding revealed in high resolution structures of the maltodextrin transport/chemosensory receptor. *Structure* **5,** 997–1015
49. Arnold, K., Bordoli, L., Kopp, J., and Schwede, T. (2006) The SWISS-MODEL workspace. A web-based environment for protein structure homology modeling. *Bioinformatics* **22,** 195–201
50. Meijer, W. H., Gidijala, L., Fekken, S., Kiel, J. A., van den Berg, M. A., Lascaris, R., Bovenberg, R. A., and van der Klei, I. J. (2010) Peroxisomes are required for efficient penicillin biosynthesis in. *Penicillium chrysogenum*. *Appl. Environ. Microbiol.* **76,** 5702–5709
51. Liu, F., Lu, Y., Pieuchot, L., Dhavale, T., and Jedd, G. (2011) Import oligomers induce positive feedback to promote peroxisome differentiation and control organelle abundance. *Dev. Cell* **21,** 457–468
52. Lingard, M. J., and Bartel, B. (2009) Arabidopsis *LON2* is necessary for peroxisomal function and sustained matrix protein import. *Plant Physiol.* **151,** 1354–1365
53. Okumoto, K., Kametani, Y., and Fujiki, Y. (2011) Two proteases, trypsin domain-containing 1 (Tysnd1) and peroxisomal lon protease (PsLon), cooperatively regulate fatty acid β-oxidation in peroxisomal matrix. *J. Biol. Chem.* **286,** 44367–44379
54. Omi, S., Nakata, R., Okamura-Ikeda, K., Konishi, H., and Taniguchi, H. (2008) Contribution of peroxisome-specific isoform of Lon protease in sorting PTS1 proteins to peroxisomes. *J. Biochem.* **143,** 649–660
55. Iyer, L. M., Leipe, D. D., Koonin, E. V., and Aravind, L. (2004) Evolutionary history and higher order classification of AAA+ ATPases. *J. Struct. Biol.* **146,** 11–31
56. Hanson, P. I., and Whiteheart, S. W. (2005) AAA+ proteins. Have engine, will work. *Nat. Rev. Mol. Cell Biol.* **6,** 519–529
57. Sauer, R. T., Bolon, D. N., Burton, B. M., Burton, R. E., Flynn, J. M., Grant, R. A., Hersch, G. L., Joshi, S. A., Kenniston, J. A., Levchenko, I., Neher, S. B., Oakes, E. S., Siddiqui, S. M., Wah, D. A., and Baker, T. A. (2004) Sculpting the proteome with AAA(+) proteases and disassembly machines. *Cell* **119,** 9–18
58. Rep, M., van Dijl, J. M., Suda, K., Schatz, G., Grivell, L. A., and Suzuki, C. K. (1996) Promotion of mitochondrial membrane complex assembly by a proteolytically inactive yeast Lon. *Science* **274,** 103–106
59. Nijland, J. G., Kovalchuk, A., van den Berg, M. A., Bovenberg, R. A., and Driessen, A. J. (2008) Expression of the transporter encoded by the cefT gene of *Acremonium chrysogenum* increases cephalosporin production in *Penicillium chrysogenum*. *Fungal Genet. Biol.* **45,** 1415–1421